Advances in electrospun carbon fiber-based electrochemical sensing platforms for bioanalytical applications

Citation: Mao, Xianwen et al. "Advances in Electrospun Carbon Fiber-Based Electrochemical Sensing Platforms for Bioanalytical Applications." Analytical and Bioanalytical Chemistry 408.5 (2016): 1307–1326.

As Published: http://dx.doi.org/10.1007/s00216-015-9209-x

Publisher: Springer Berlin Heidelberg

Persistent URL: http://hdl.handle.net/1721.1/107163

Version: Author's final manuscript: final author's manuscript post peer review, without publisher's formatting or copy editing

Advances in Electrospun Carbon Fiber-Based Electrochemical Sensing Platforms for Bioanalytical Applications

*Xianwen Mao, Wenda Tian, T. Alan Hatton, Gregory C. Rutledge**

Department of Chemical Engineering, Massachusetts Institute of Technology, 77 Massachusetts Avenue, Cambridge, Massachusetts, 02139, USA

*Corresponding author, E-mail: rutledge@mit.edu

((Note to vendor, for copy editing: Please do not change the footnote))

Published in the topical collection *Fiber-based Platforms for Bioanalytics* with guest editors Antje J. Baeumner and R. Kenneth Marcus.

Abstract

Electrochemical sensing is an efficient and inexpensive method for detection of a range of chemicals of biological, clinical and environmental interest. Carbon materials-based electrodes are commonly employed for the development of electrochemical sensors, due to their low cost, biocompatibility, and facile electron transfer kinetics. Electrospun carbon fibers (ECFs), prepared by electrospinning of a polymeric precursor and subsequent thermal treatment, have emerged as promising carbon systems for biosensing applications since the electrochemical properties of these carbon fibers can be easily modified by processing conditions and post-treatment. This review addresses recent progress in the use of ECFs for sensor fabrication and analyte detection. We focus on the modification strategies of ECFs and identification of the key components that impart the bioelectroanalytical activities, and point out the future challenges that must be addressed

in order to advance the fundamental understanding of the ECF electrochemistry and to realize the practical applications of ECF-based sensing devices.

Key words: electrochemistry, biosensor, carbon fiber, electrospinning

Abbreviations

Adenine (A)
Ascorbic acid (AA)
Cellulose acetate (CA)
Chronoamperometry (CAm)
Catechol (CC)
Carbon nanofibers (CNFs)
Carbon nanofibers obtained at a pyrolysis temperature of X (CNFX)
Carbon nanotube CNT
Carbon paste electrodes (CPE)
Cytochrome *c* (cyt *c*)
Dopamine (DA)
Direct electron transfer (DET)
Differential pulse voltammetry (DPV)
Density of electronics states (DOS)
Electrospun carbon fibers (ECFs)
Electron energy loss spectroscopy (EELS)
Fermi level (E_F)
Electroactive surface area (ESA)
Guanine (G)
Glassy carbon (GC)
Glassy carbon electrode (GCE)
Gerischer-Marcus (GM)
Glucose oxidase (GOx)
Graphitized fibers (GFs)
Heterogeneous electron transfer (HET)
Hydroquinone (HQ)
Horse radish peroxidase (HRP)
Apparent electron transfer rates (k^0_{app})
Ionic liquids (ILs)
Laccase (Lac)
Limits of detection (LOD)
Magnetic glass carbon electrode (MGCE)
Nitrogen-doped carbon fibers (NCNFs)
Nickel nanoparticle loaded carbon nanofibers (NiCNFs)
Nanoparticle (NP)

Oxygen reduction reactions (ORRs)
Poly(amic acid) (PAA),
Polyacrylonitrile (PAN)
Polybenzimidazol (PBI)
Polydopamine (PDA)
Polyimide (PI)
Poly(vinyl alcohol) (PVA)
Polyvinylpyrrolidone (PVP)
Scanning electron microscopy (SEM)
Square-wave voltammetry (SWV)
Transmission electron microscopy (TEM)
Uric acid (UA)
Ultraviolet photoelectron spectroscopy (UPS)
X-ray absorption near edge spectroscopy (XANES)
X-ray photoelectron spectroscopy (XPS)
X-ray diffraction (XRD)

1. Introduction

The molecular and biomolecular electrochemistry of carbon materials, particularly their electron transfer properties, have attracted much interest for their applications in electrochemical sensing [1-3]. Relative to other materials, carbon-based electrochemical sensors enjoy several advantages, such as high sensitivity, reproducibility, low-cost, and ease of device fabrication, and therefore have been used in many practical applications in chemical and biological industries, including food quality control, bioprocessing, water treatment, and clinical chemistry. Structural modification of carbon-based sensing materials to manipulate their crystalline, electronic and chemical properties is important for enhancing sensitivity and imparting selectivity towards certain analytes. There is a wide range of methods available for structural modulation of carbon materials, such as photochemical reactions [4], diazonium ion modification [5], noncovalent modification using metallocenes [6, 7], pyrenes [8-10], or porphyrins [11-13], and electrochemical precipitation of conducting polymers [14, 15].

Carbon fibers have attracted attention since the late 1950s, when Bacon produced the first high performance carbon fibers [16]. The conventional methods to fabricate carbon fibers include chemical vapor deposition and pyrolysis of fibers spun from organic precursors [17]. Electrospinning followed by pyrolysis has recently emerged as an efficient, versatile and inexpensive strategy to fabricate ultrafine carbon fibers [18]. Control over surface chemistries and microstructures of electrospun carbon fibers (ECFs) is usually achieved through variation of solution and processing parameters [19, 20] and adjustment of spinning set-up geometries [21]. Complicated fibrous structures, such as core–shell [21, 22], porous [23], and multi-channel fibers [24], can be realized by co-

spinning different solutions with customized spinnerets. Previous reviews on the applications of ECF-based systems have mainly concentrated on electrochemical energy storage, gas storage, polymer reinforcement, and membrane separation [18-25].

Herein we provide an overview of ECF-based electrochemical sensing materials and their applications in detection of biologically relevant molecules. The electrochemical sensing properties of other types of carbon materials, including carbon nanotubes [26, 27], graphene [2, 28], and conventional carbon electrodes (e.g., graphite and glassy carbon) [29-31] have been discussed in several earlier reports. In this article, following a brief discussion on the preparation and characterization of ECFs, we review the modification strategies of ECFs and the applications of the resulting materials in bioelectroanalysis, as well as point out the future challenges that must be addressed in order to gain a deeper understanding of the ECF electrochemistry and realize the practical applications of ECF-based devices.

2. Electrospun Carbon Fiber-Based Sensing Materials

The often-cited advantages of electrospinning include ease of operation, cost-effectiveness, high efficiency and yield, and reproducibility of the resulting materials properties. The versatility of electrospinning is reflected in the diverse nature of materials that are electrospinnable, as well as the different forms of fiber assemblies and architectures that have been produced. A conventional electrospinning set-up is illustrated schematically in **Figure 1A** [32]. This basic electrospinning set-up consists of three essential components: a spinneret (e.g., a syringe), a high voltage supply, and a low voltage (e.g. grounded) collector. A drop of a viscoelastic polymer solution on the tip of a

spinneret is charged by the high voltage supply. The repulsive electrical forces among the charges on the surface of the drop compete with the surface tension force that stabilizes the drop. Once the applied electric potential reaches the critical value at which the surface charge repulsion overcomes surface tension, a charged jet is emitted from the drop, which fluid is replenished by the spinneret. The ejected jet accelerates downfield towards the collector, and its diameter decreases due to charge repulsion and electrical stresses that arise due to the applied electrical field. The presence of surface charges in an applied electric field gives rise to a "whipping" instability, in which spontaneous deviations of the jet from the axis of flow (i.e. bending) are amplified, which results in further stretching of the liquid filament. As the solvent evaporates, solidified continuous polymer fibers are generated on the grounded collector. The diameters of electrospun fibers can be controlled to be in the nanometer to micrometer range. An alternative technique with potential large scale production capabilities is "free-surface" electrospinning (**Figure 1B**), where jets can be generated from free liquid surfaces such as films, drops or bubbles, without the need for a spinneret [33, 34].

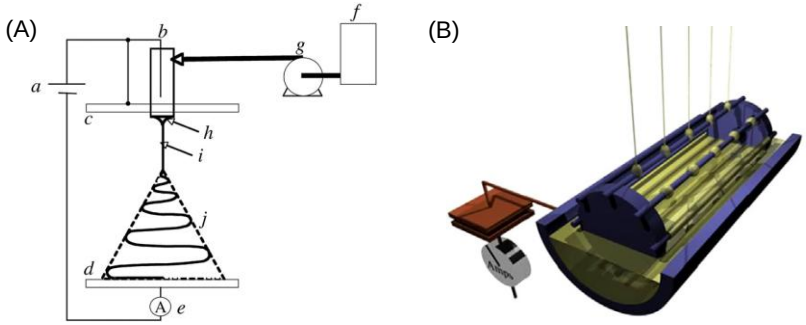

Figure 1. (A) Schematic illustration of a conventional electrospinning set-up: (a) power supply (usually with high voltage capabilities up to 30 kV); (b) charging device; (c) electrode charged to a high potential (e.g. flat plate); (d) grounded electrode or collector (e.g. flat plate); (e) device for current measurements; (f) fluid reservoir; (g) flow rate control; (h) cone; (i) thinning jet; (j) whipping instability region. Reprinted with permission from ref 32. (Copyright Elsevier, 2007.) (B) An example of free surface

electrospinning. Conductive wires are used as the high voltage electrodes. The fluid reservoir (gold) is also charged to a high voltage. As the spindle of wires rotates counterclockwise (as viewed here), the precursor polymer solution first forms a liquid film as shown on the first (leftmost) wire, which then breaks up into droplets as shown on the second (middle) wire. The electric field at the wire increases as the spindle rotates, resulting emission of a liquid jet as shown on the third (rightmost) wire. Dry fibers form as the solvent evaporates. Reprinted with permission from ref 34. (Copyright Elsevier, 2013.)

More than a hundred types of polymers have been electrospun; among them, those with high carbon yields (i.e., the ratio between the mass of carbonized fibers to the mass of polymer fibers prior to carbonization) can be used to produce electrospun carbon fibers. The main types of electrospinnable polymers with high carbon yields are polyacrylonitrile (PAN), poly(vinyl alcohol) (PVA), cellulose acetate (CA), polyvinylpyrrolidone (PVP), polyimide (PI), polybenzimidazol (PBI), poly(amic acid) (PAA), phenolic resin, and pitch [18, 35]. The generation of carbonaceous fibers from precursor polymer fibers generally involves two steps: (i) stabilization at relatively low temperatures (200 – 300 °C) in an oxidative environment to convert thermoplastic polymer fibers to condensed thermosetting fibers, and (ii) carbonization at high temperatures (usually around 800 – 1300 °C) in an inert gas atmosphere such as nitrogen or argon to removes heteroatoms. The fabrication process of ECFs is flexible and versatile in that it is easy to manipulate the composition of the precursor solution and to adjust the thermal treatment conditions. The post-treatment of ECFs using a variety of carbon surface functionalization methods can also introduce foreign active components to the fibers. The morphological characterization of ECF-based sensing materials is usually performed using transmission electron microscopy (TEM) and scanning electron microscopy (SEM). Nitrogen adsorption/desorption isotherm measurements can be used to determine the specific surface area and pore size distributions of ECFs [36, 37]. Useful

structural information on the carbonized fibers relevant to their electrochemical sensing performance (*e.g.*, the defect concentration, surface chemistry, and electronic structure) can be obtained from various spectroscopic techniques, such as X-ray photoelectron spectroscopy (XPS), electron energy loss spectroscopy (EELS), ultraviolet photoelectron spectroscopy (UPS), X-ray absorption near edge spectroscopy (XANES) and Raman spectroscopy. The chemical, morphological and electronic properties of ECFs depend on a number of factors, such as the type of polymer precursor, the electrospinning conditions, the thermal treatment temperature, and the chemical modification procedures. For example, PAN-derived carbon fibers usually exhibit turbostratic carbon structures with an interlayer distance of ~ 0.37 nm, whereas pitch-derived carbon fibers display a higher degree of graphitization with an interlayer distance of ~0.34 nm, consistent with that for graphite. The electrospinning conditions, including the concentration of the polymer solution, flow rate, voltage applied and humidity, affect the diameter of the resulting fibers and the specific surface area of the fiber mat. It is possible to manipulate the pore size distribution of the ECFs by varying the chemical composition of the electrospinning solution, changing the carbonization temperature, and using additional activation steps (e.g., steam treatment). Surface modification, such as controlled oxidation and doping with heteroatoms, can be used to modulate the electronic structure of ECFs. For a thorough summary of the fundamental properties of ECFs fabricated and treated under different conditions, see the review by Inagaki *et al.* [18].

ECF-based sensing systems have been applied to the detection of a range of biologically relevant molecules, the chemical structures of some of which are summarized in **Figure 2**. The detection of aromatic molecules containing hydroxyl

groups is of practical importance in environmental protection and medicine. Catechol and hydroquinone are widely used in cosmetic dyes, pesticides, and pharmaceuticals, but are highly toxic and not easily degradable, posing serious environmental concerns [38]. Dopamine is an important neurotransmitter, the abnormal level of which is closely associated with Parkinson's disease, Alzheimer's disease, and schizophrenia [39, 40]. The detection of ascorbic acid and uric acid plays an important role in laboratory medicine. Paracetamol is one of the common ingredients in over-the-counter analgesics and antipyretics, and can cause liver cell and renal cell necrosis if it is overdosed [41]. Hydrogen peroxide is an effective disinfecting agent and a byproduct of various oxidase enzymes, the concentration of which can be used as an indicator for tracing the progress of biochemical reactions [40, 42, 43]. Hydrazine has been used in rocket fuels and as a precursor for pharmaceuticals; the detection of hydrazine is crucial because even short-time exposure to it can result in severe adverse effects on human health [44]. Glucose and other sugars (fructose and sucrose) are commonly found in fruits and food; the level of glucose is important for the diagnosis and treatment of diabetes [41, 45]. **Table 1** summarizes the key components of ECF-based electrochemical sensors, the types of analytes that can be detected using these sensors, the electrochemical techniques used for sensing, and the performance parameters of these sensors (i.e., limit of detection and dynamic range).

The development of ECF-based sensing materials for electrochemical detection of biologically relevant molecules relies on three main strategies: (i) manipulation of carbonization conditions or doping with heteroatoms to modulate the electrochemical properties of carbon fibers, (ii) incorporation of electrochemically active metal

nanoparticles into ECFs by adjusting the composition of the precursor solution, and (iii) post-modification of ECFs using solution-based chemical processes. In the following three subsections, we discuss the sensing performance of ECF-based electrochemical systems, classified into these three categories. These strategies generally enhance the electron transfer efficiencies between redox-active systems and the electrode materials. In addition to the target molecules listed in **Table 1**, sensing devices based on ECFs can be potentially applied to a great variety of other redox-active analytes that are of importance in chemical, biological, environmental and pharmaceutical, industries, such as dyes, heavy metals, proteins, DNAs, drugs, and pesticide residuals [27, 46-49].

For the development of sensing devices, in most cases, the ECFs, with or without post-modification, are milled to break up the fibers, and then mixed with polyelectrolyte binders dissolved in solvents, followed by drop-casting of the ECF-containing suspension with known fiber concentrations onto a substrate electrode. Alternatively, free-standing ECF mats have also been used directly as sensing electrodes without the need for a supporting substrate. Throughout this article, the nomenclature "fiber-A/B//substrate" is used to identify a multi-component sensing device, where "-" means that ECFs are tightly bonded with component A (e.g., Pd-ECF indicates Pd-loaded ECFs), and "/" means that fibers are physically mixed with component B (e.g., ECF/Nafion indicates that ECFs are physically mixed with Nafion).

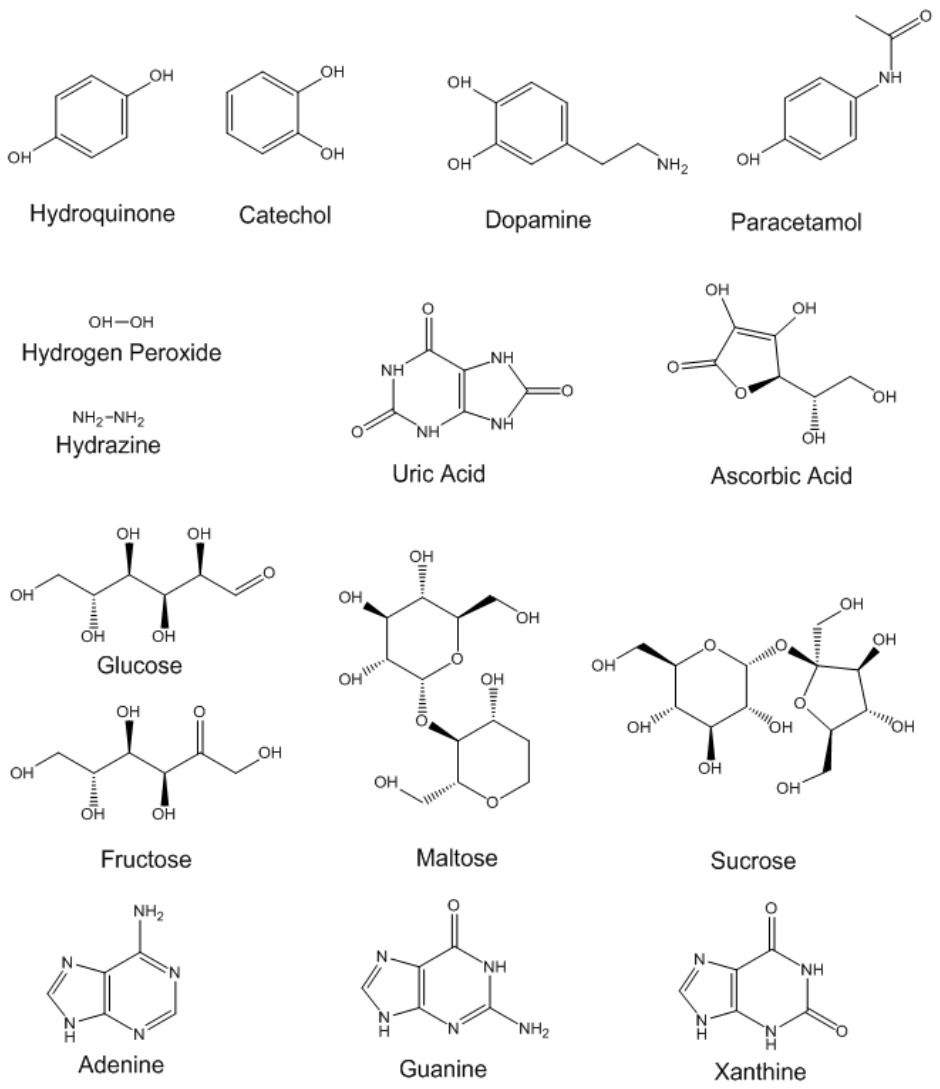

Figure 2. The chemical structures of a range of biologically relevant molecules that can be detected by ECF-based sensing systems: hydroquinone, catechol, dopamine, paracetamol, hydrogen peroxide, hydrazine, uric acid, ascorbic acid, glucose, fructose, maltose, sucrose, adenine, guanine, and xanthine.

Table 1. Summary of the target analytes, the key components and the performance parameters (LOD and dynamic rang) of various ECF-based electrochemical sensors, and the method used for detection.

Year	Analyte	Key Components of Sensor	LOD [μM]	Dynamic Range [μM]	Method for Detection	Ref.
2015	catechol	Magnetic polydopamine-laccase-nickel nanoparticle-loaded ECF	0.69	1- 9100	CV	[50]

		composite				
2014	catechol	Electrospun copper/carbon composite nanofibers	1.18	9.95- 9.76	CAm	[51]
2014	catechol	ECFs blended with laccase and Nafion	0.63	1 –1310	CV, CAm	[52]
2012	catechol, hydroquinone	ECF-modified carbon paste electrode	0.2	catechol: 0.2; hydroquinone: 0.4	CV, DPV	[38]
2014	dopamine	ECF decorated with Ag−Pt Bimetallic Nanoparticles	0.11	10 – 500	CV DPV	[40]
2014	dopamine	Screen-printed carbon electrode functionalized with graphene nanoparticle-loaded ECFs	0.07	0.5 – 100	CV, EIS, SWV	[39]
2014	dopamine	Continuous all-carbon ECFs	0.07	0.2 – 700000	DPV, CV	[53]
2010	dopamine, ascorbic acid, uric acid	Composite of ECFs and ionic liquid	NA	NA	CV	[54]
2010	hydrazine	Rhodium nanoparticle-loaded ECFs	0.3	0.5 – 175	CV, CAm	[44]
2013	hydrogen peroxide	ECFs with manganese dioxide nanoparticles	1.1	10 – 15000	CV, CAm	[42]
2013	hydrogen peroxide	ECFs decorated with platinum nanoparticles	3.4	10 – 15000	CV, CAm	[55]
2012	hydrogen peroxide	ECF web with horseradish peroxidase	1.3	1 – 10	CAm	[56]
2011	hydrogen peroxide	Pt nanoparticle-loaded ECFs	0.6	1 – 800	CV	[57]
2011	hydrogen peroxide, β-NADH	Pd-carbon composite fibers prepared by electrodepositing Pd onto ECFs	NA	NA	CV	[58]
2008	hydrogen peroxide, NADH	Palladium nanoparticle-loaded ECFs	H_2O_2: 0.2; NADH: 0.2	H_2O_2: 0.2 - 20000; NADH0.2 - 716.6	EIS, CV	[59]
2015	paracetamol, glucose	$Ni(NO_3)_2$-loaded ECFs	paracetamol 2.75; glucose: 0.05;	39.8 – 135.6	CV	[41]
2014	glucose	Free-standing nitrogen-doped ECFs	15	200 − 1200 at −0.42 V; 50 − 3000 at 0.40 V	CV	[60]
2009	glucose	Ni nanoparticle-loaded ECFs	1	2 – 2.5	CV	[45]
2011	xanthine	ECF-modified carbon paste electrode	0.02	0.03 – 21.19	CAm	[61]
2015	adenine, guanine	Ni loaded ECFs	0.03	0.05 - 2	CV, DPV	[62]

2.1 ECFs with or without Dopants

In this section, we discuss the performances of electrochemical sensors that consist of ECFs without additional functional components such as metal nanoparticles. In

these sensors, generally the properties of the carbon component govern the electrochemical activities towards redox-active molecules.

PAN-derived ECFs, without any additional modifications, were used directly to detect hydroquinone (HQ) and catechol (CC) simultaneously [38]. **Figure 3A** shows differential pulse voltammetry (DPV) responses on an ECF-modified carbon paste electrode (CPE) when the concentration of CC was varied from 1 to 200 μM in 0.1 M PBS (pH 7.0), while the HQ concentration was fixed at 50 μM. With an increasing CC concentration while holding HQ concentration constant, the anodic DPV peaks increased monotonically, which indicates that the oxidation of HQ and CC on ECF//CPE took place independently. Based on the DPV measurements, the dynamic range for detection of CC was 1 – 200 μM, and the limit of detection was determined to be 0.2 μM. **Figure 3B** shows the DPV responses on this electrode for different concentrations of HQ while keeping the CC concentration constant at 50 μM. It was observed that the peak current corresponding to oxidation of HQ increased with HQ concentration, whereas the peak current corresponding to oxidation of CC remained almost unchanged. The dynamic range for detection of HQ in the presence of CC was 1 – 200 μM, with a detection limit of 0.4 μM. PAN-derived ECFs were also used for simultaneous detection of the mixture of dopamine (DA), ascorbic acid (AA) and uric acid (UA), and the mixture of guanine (G) and adenine (A) [54]. In this study, the authors used ionic liquids (ILs) as the binder for the ECFs to fabricate the sensors, although the role of ILs in the sensing performance is not clear. These two studies [38, 54] have demonstrated that as-synthesized PAN-derived ECFs exhibit high electrochemical activities towards detection of certain redox-active species. However, the effects on the sensing performance of one important factor

in the synthesis of ECFs, that is, the thermal treatment condition, was not examined. Also, the relationship between the microstructures of carbon fibers and the observed sensing capabilities was not investigated.

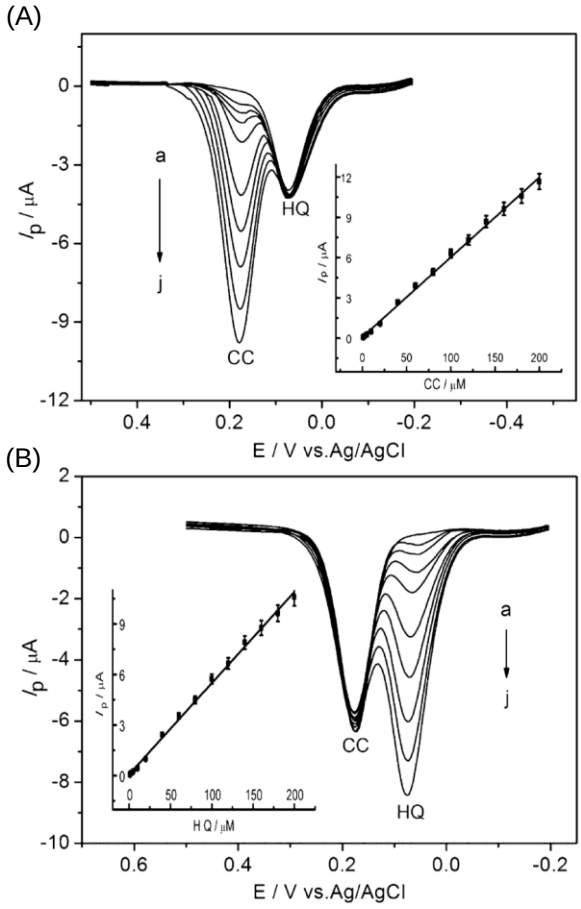

Figure 3. DPVs for ECF-CPE in (A) different concentrations (a-j: 1, 2, 5, 10, 40, 80, 120, 160, 200 μM) of CC containing 50 μM HQ and (B) different concentrations (a-j: 1, 2, 5, 10, 40, 80, 120, 160, 200 μM) of HQ containing 50 μM CC. Insets show the calibration plots of CC and HQ. Reprinted with permission from ref 38. (Copyright Elsevier, 2012.)

Recently, Mao *et al*. studied the relationship between the carbonization temperature and the microstructural and electrochemical properties of PAN-derived ECFs [56]. In this study, carbon nanofibers obtained at a pyrolysis temperature of 1000, 1100 or 1200 °C were denoted as ECF1000, ECF1100, and ECF1200, respectively. **Figure 4**

shows evidence of control over the surface chemistries and electronic structure of these ECFs through changes in the carbonization temperature. The XPS C 1s spectra for ECF1000, ECF1100, and ECF1200 are shown in **Figure 4A**. It can be observed that with a higher carbonization temperature the peak position in the spectrum was located at a lower binding energy. This observation suggests that the sp^2/sp^3 ratio of these carbon fibers increased with the pyrolysis temperature, because the sp^2 bond has a lower binding energy compared to the sp^3 bond. Quantitatively, the sp^2/sp^3 ratio, calculated from deconvolution of the C 1s spectra, increased from ECF1000 (1.07) to ECF1100 (1.17) to ECF1200 (1.41). Based on the Raman spectra (**Figure 4B**), it was concluded that a higher carbonization temperature resulted in a higher graphite concentration, in that the R_I ratio (the ratio of the peak intensity of the D band to the peak intensity of the G band) decreased with the pyrolysis temperature. A smaller R_I ratio suggests higher sp^2 content for carbonaceous materials [63].

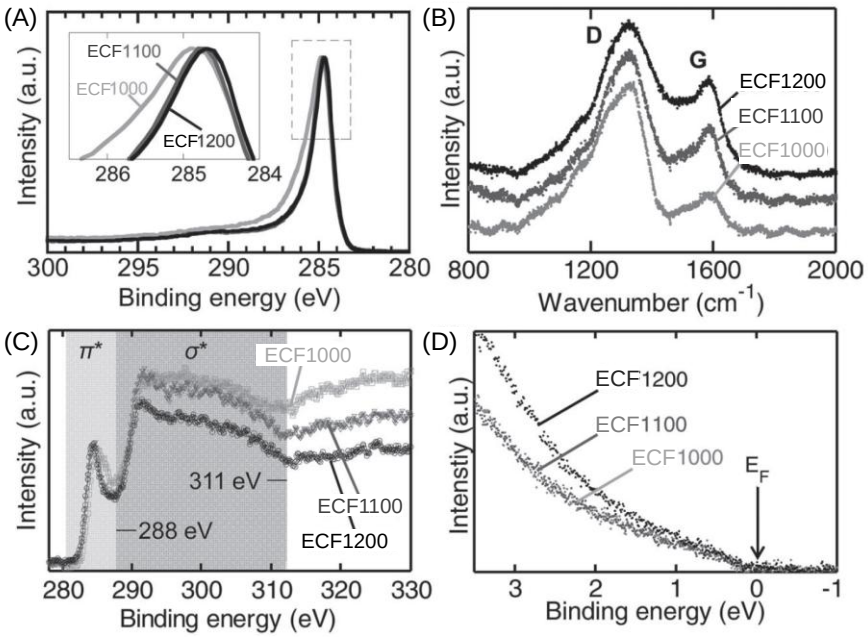

Figure 4. Effect of carbonization temperature on the nanographite concentration and density of states for the ECF webs. (A) High resolution C 1s spectra (inset:

magnification of the dotted rectangular area). (B) Raman spectra. (C) EELS spectra. (D) UPS spectra showing the density of electronic states near the Fermi level. Reprinted with permission from ref 56. (Copyright John Wiley and Sons, 2013.)

For carbonaceous materials, the density of electronics states (DOS) near the Fermi level (E_F), particularly the density of π electronic states, dictates the electrochemical activities [64]. Therefore, electron energy loss spectroscopy (EELS) and UPS were employed to probe the conduction and valence band structures, respectively. EELS spectra (**Figure 4C**) can be used to investigate the π and σ orbitals of ECFs; excitation of electrons to the π^* and σ^* states results in the peak from 280 to 288 eV and the broad band from 288 to 311 eV, respectively [65]. The π/σ ratio increased from 0.10 to 0.12 to 0.14 for ECF1000, ECF1100 and ECF1200, respectively, indicating that a higher treatment temperature resulted in a higher density of π states. The UPS spectra near the Fermi level normalized by the total integrated intensities are shown in **Figure 4D**, from which it can be seen that the density of π electronic states (that is, the DOS near E_F) for ECF1200 is markedly higher than those for ECF1100 and ECF1000, whereas the latter two systems exhibit densities of states that are nearly indistinguishable.

McCreery [1] has suggested that redox-active systems be categorized into four different classes, based on how the electron transfer kinetics are affected by surface conditions of electrodes. These different classes of redox species are termed (i) outer-sphere, (ii) oxide-sensitive, (iii) adsorption-assisted, and (iv) surface-sensitive but not affected by oxide or adsorption. In the study by Mao *et al*., four redox couples were selected, $Ru(NH_3)_6^{3+/2+}$, $Fe^{3+/2+}$, dopamine, and $Fe(CN)_6^{3-/4-}$, which are typical examples from each of these four classes. It was found that the apparent electron transfer rates (k^0_{app}) for the four redox species increased from ECF1000 to ECF1100 to ECF1200, suggesting that the strategy of controlling electron transfer kinetics through manipulation

of the DOS is effective, and is a general method that can be applied to different classes of redox systems. Furthermore, it was found that the ECF system with a high DOS, i.e. ECF1200, exhibited high direct electron transfer (DET) efficiencies with cytochrome *c* (cyt *c*), which is a DET-type redox-active enzyme that has been studied extensively [66]. Conventional carbon electrodes such as graphitized fibers, glassy carbon electrodes, and carbon paste electrodes usually exhibit negligible electrochemical response towards cyt *c*. A second DET-type enzyme, horse radish peroxidase (HRP), was immobilized onto ECF1200; the HRP-modified ECF1200 (HRP/ECF1200) electrode exhibited bioelectrocatalytic activities towards detection of hydrogen peroxide. From steady-state amperometric measurements, the H_2O_2 detection limit of HRP/ECF1200 was estimated to be 1.3 μM.

In another report, PAN-derived ECFs were mixed with laccase and Nafion for the development of enzymatic biosensors for the detection of catechol (CC) [52]. The sensing performance of the laccase/Nafion/ECF sensor was evaluated by chronoamperometry. **Figure 5A** displays the steady-state current response of this sensor upon introduction of different concentrations of CC into an acetate buffer solution (pH = 5.5). The first significant current response was observed upon addition of 20 nM CC into the buffer solution. The inset in **Figure 5A** shows that 95% of the steady-state current value was obtained within two seconds,, indicating the rapid response of the sensor toward CC. **Figure 5B** shows that the steady-state current values continued to increase with the successive addition of CC. The inset in **Figure 5B** shows the calibration curve, from which it can be seen that the linear range was 1 – 1310 μM, much broader than that for the previously developed sensor consisting of laccase-modified carbon nanotubes

(CNTs) [67]. The laccase/Nafion/ECF sensor had a limit of detection of 0.63 μM, a sensitivity of 41 $\mu A \cdot mM^{-1}$, and a Michaelis–Menten constant of 50.64 μM, which was calculated from the electrochemical version of the Lineweaver–Burk plot [68].

ECF free of dopants has also been used for detection of xanthine, a purine base, the detection of which is crucial in clinical diagnosis and water quality monitoring. Distinguished by its high electrocatalytic activity and fast amperometric response, this ECF-based amperometric sensor could detect xanthine at a concentration as low as 20 nM, with a dynamic linear range of 0.03-21.19 μM [61].

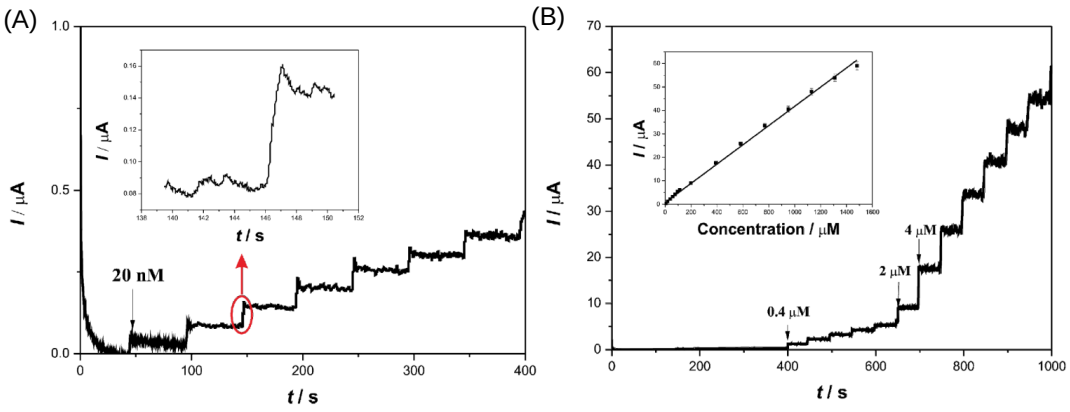

Figure 5. (A) A representative chronoamperometric profile (up to 400 s) of laccase/Nafion/ECFs//GCE when catechol solutions were added to an acetate buffer solution under constant stirring. Inset: enlarged red circle showing the third addition of catechol. (B) The chronoamperometric profile (up to 1000 s) of laccase/Nafion/ECFs//GCE with the inset showing the linear correlation between the current magnitude and the catechol concentration. Reprinted with permission from ref 52. (Copyright Beilstein-Institut, 2014.)

Liu *et al.* reported preparation of nitrogen-doped electrospun carbon fibers (N-ECFs) from the thermal treatment of electrospun PAN fibers [60]. The key step to incorporate N atoms into the carbon fibers was stabilization in a mixture of NH_3 and air at 300 °C for

60 min. The control sample, ECFs without dopamine, was prepared by stabilization in air. Modification of carbon materials with heteroatoms is expected to result in more defective sites on the surface [69]. The Raman spectra (**Figure 6A**) show that the R_I value of N-ECFs (1.942) was larger than that of ECFs (1.850), indicating that N-ECFs contained more defects. While XPS survey scans (**Figure 6B**) show that N-ECFs contained less N content than did ECFs, previous studies demonstrate that the catalytic activity of nitrogen-doped carbons is related to the forms of N-containing groups, rather than the nitrogen content itself [70]. The high-resolution N 1s spectra of ECFs and N-ECFs are shown in **Figure 6C and 6D**, respectively. The N spectra can be deconvoluted into three different forms: graphitic-N (401.4 ± 0.3 eV), pyrrolic-N (400.4 ± 0.3 eV), and pyridinic-N (398.7 ± 0.3 eV) [71, 72]. Pyrrolic-N at the edges of graphene layers would show higher charge mobility and better donor−acceptor properties than pyridinic-N and graphitic-N [73]. Based on the N 1s spectra, the content of pyrrolic-N was higher in N-ECFs (42%) than in ECFs (23%). Therefore N-ECFs should exhibit higher electrocatalytic activities than do ECFs. In this study, the authors found that, compared to ECFs, N-ECFs exhibited faster electron transfer kinetics with various redox probes, and showed a higher catalytic activity for the oxygen reduction reaction. When the N-ECFs were modified with glucose oxidase (GOx) to fabricate glucose sensors, the resulting sensor was shown to exhibit a dynamic range from 0.2 to 1.2 mM and a limit of detection of 0.06 mM.

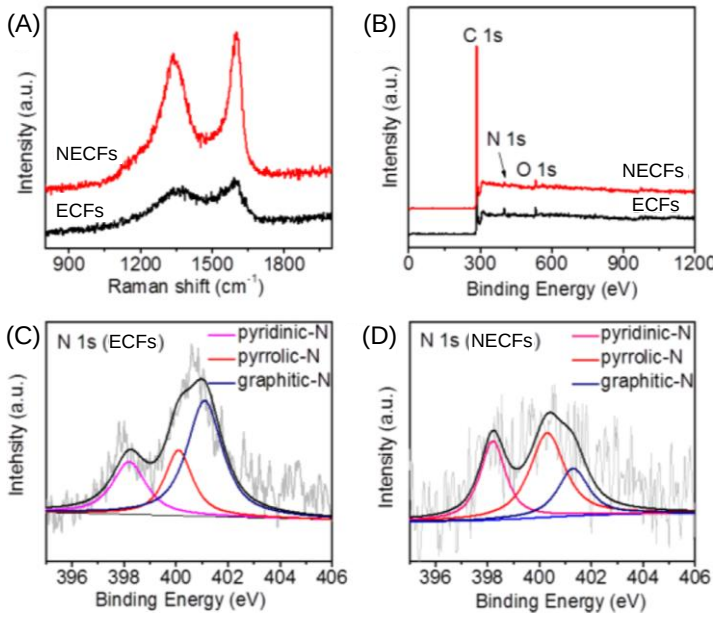

Figure 6. (A) Raman spectra and (B) XPS survey scans of ECFs and N-ECFs. The high resolution N 1s spectra of (C) ECFs and (D) N-ECFs. Reprinted with permission from ref 60. (Copyright American Chemical Society, 2014.)

For electrochemical sensors based on carbon materials, most previous efforts have concentrated on the improvement of limits of detection [1, 27, 46, 47, 74-77]. However, very few reports have focused on the range of detection, another important aspect for evaluating the sensing performance. Analysis of undiluted, 'real world' samples that span a broad range of concentrations requires the use of sensors with wide-range detection capabilities. Such sensors may be particularly useful for applications such as analysis of water quality [46], food regulation [49], pharmaceutical analysis [48], and *in vivo* sensing in biological media [78-80]. The factor that determines the upper bound of the detection range of an electrochemical sensor is the electroactive surface area (ESA). An increase in ESA postpones current saturation to higher analyte concentrations, resulting in a higher upper bound to the dynamic range. However, mainly because of their limited ESAs, most sensors based on carbon electrodes display narrow detection ranges. Traditional carbon

electrode systems, including microfabricated carbon films, carbon paste electrodes, and glassy carbon electrodes, display structures of low porosity, and thus usually have small active surface areas [1]. A possible way to increase ESAs is through deposition of CNT or graphene dispersions onto flat electrodes to generate porous architectures. However, this method requires proper, sometime complicated, assembly processes to integrate discontinuous CNTs or graphene onto substrates.

In a recent study, the unique ability of electrospinning to produce continuous fibers has been exploited to fabricate all-carbon electrochemical sensors with high ESAs and thus wide dynamic ranges [53]. The schematic illustration of the sensor fabrication procedure is shown in **Figure 7A**. First, a thin PAN film was deposited onto a conductive substrate via spin-coating. Next, PAN nanofibers were electrospun onto the polymer film on the substrate. The polymer film between the substrate and the fibers functioned as an adhesive layer in order to prevent fiber detachment from the substrate after carbonization. The substrate was a Toray carbon paper consisting of graphitized microfibers, chose for its stability during high temperature treatment. The subsequent step was carbonization of the PAN fibers together with the PAN film at a temperature of 1200 °C. PAN-derived ECFs carbonized at this temperature had been reported previously to exhibit high densities of electronic states and strong electrocatalytic activities towards a variety of redox-active molecules [56].

Scanning electron microscopy (SEM) imaging shows that the average diameters of as-spun polymer fibers were around 300 nm (**Figure 7B**). After carbonization, because of the mass loss due to polymer degradation, the resulting carbon fibers had smaller diameters of around 250 nm (**Figure 7C**) [81]. SEM cross-sectional analysis shows that

ECFs seemed to be interconnected without the use of binders, and firmly attached to the substrate (**Figure 7D, E**). Additionally, it was observed that the thickness of the ECF mesh increased from ~60 to ~500 μm when the electrospinning time was increased from 12 to 68 h. This observation suggests that the quantity of the electroactive carbon fibers integrated on the substrate could be varied simply by using different deposition times. The capability of modulating the loading of ECFs allows for systematic adjustment of ESA, providing an opportunity to achieve wide range detection of redox-active analytes. Moreover, unlike most sensors fabricated from as-synthesized CNTs or graphene, the high electrocatalytic activities of these ECF sensors are readily obtained by thermal treatment at 1200 °C, without further modification or activation steps or the need for other, non-carbon ingredients.

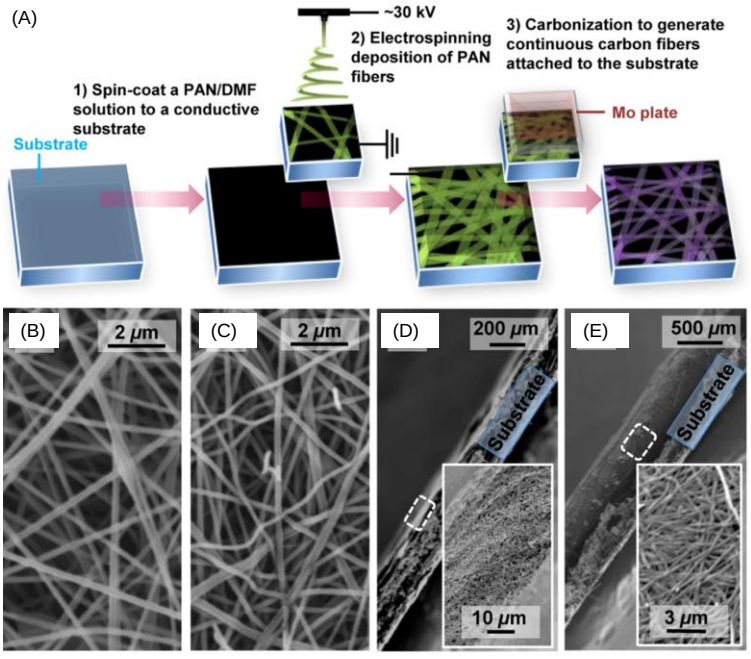

Figure 7. (A) Schematics of the fabrication procedure of an ECF sensor. (B, C) SEM images of (B) as-spun polymer fibers and (C) carbonaceous fibers after thermal treatment. (D, E) Cross-sectional SEM images of the ECF sensors with an electrospinning

deposition time of (D) 12 and (E) 68 h. Insets: magnification of the dotted rectangular areas. Reprinted with permission from ref 53. (Copyright American Chemical Society, 2014.)

The performance of the ECF sensors was evaluated using dopamine as the model analyte to be detected. A variety of carbon electrodes have been used for dopamine sensing, and thus the sensing properties of the ECF sensors can be compared with those of previously reported sensing devices. The sensor composed of substrate-supported continuous ECFs, prepared by 12 hrs of electrospinning deposition, exhibited an extremely wide dynamic range for DA detection (0.2 to 700,000 μM) and a detection limit (0.08 μM) that is comparable to, or better than, the sensitivities of many sensors based on carbon nanotubes [82-93] or graphene [94-100].

2.2 Metal Nanoparticle-Decorated ECFs

In this section, we discuss metal nanoparticle (NP)-decorated ECFs prepared by varying the composition of the precursor solution prior to electrospinning. Easy incorporation of metal nanoparticles is another advantage of the fabrication process based on electrospinning. The general procedure is to dissolve metal salts into the precursor polymer solution, and convert the metal salt to metal nanoparticles during the thermal treatment. Therefore, this NP incorporation process is not restricted to the defect sites on the surface of ECFs, which is an important requirement for the deposition of metallic nanoparticles onto carbon nanotubes and other types of carbon fibers [101-103]. In most cases, the metal nanoparticles are the active components that impart electrocatalytic activities, and the NP-ECF hybrids can function as non-enzymatic sensors for analytes that are usually detectable by redox enzymes.

Pd-ECF hybrids were prepared by thermal treatment of electrospun PAN-Pd(acetate)$_2$ (Pd(Ac)$_2$) composite nanofibers [59]. The fibers were electrospun from a precursor polymer solution with the dissolved metal salt (4.8 wt% Pd(Ac)$_2$ and 8 wt% PAN in DMF). The thermal treatment consisted of three steps: stabilization of PAN fibers in air at 230 °C, reduction of Pd^{2+} in H_2/Ar mixture at 300 °C, and carbonization of PAN fibers in Ar at 1100 °C. X-ray diffraction (XRD) (**Figure 8A**) confirms that the metallic Pd phase was generated in the Pd-CNF hybrids. The diffraction peaks labelled with Pd shown in this figure could be indexed to the cubic phase of Pd, while diffraction peaks close to 26°, 42°, 44°, 59° and 77° were assigned to the (002), (100), (101), (103), and (110) planes of graphite (JCPDS, No. 13-0148), respectively. The interlayer spacing in Pd-ECF (d_{002} = 0.341 nm) was bigger than the value for graphite (0.335 nm), indicating the turbostratic nature of these carbon fibers [104]. The effective incorporation of Pd NPs could be visualized by SEM images (**Figure 8B, 8C**), which show that the Pd NPs were either deposited on the fiber surface or embedded inside these fibers. TEM analysis (**Figure 8D**) shows well-dispersed spherical Pd nanoparticles with an average diameter of ~70 nm.

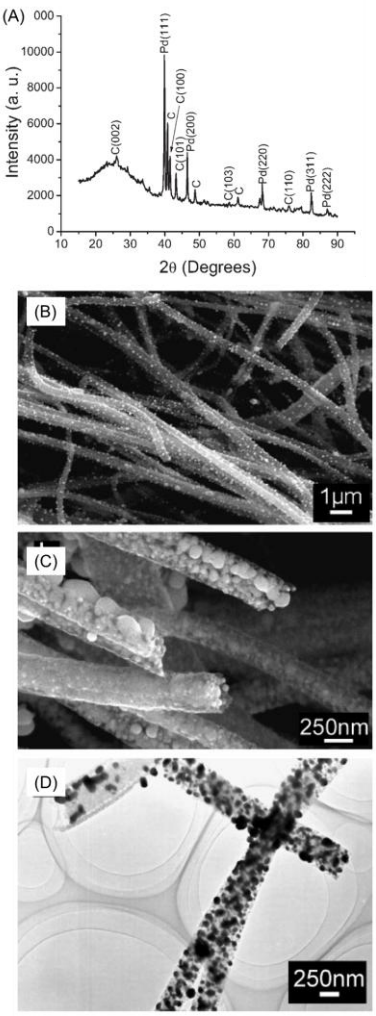

Figure 8. (A) XRD pattern, (B) SEM image, (C) high magnification SEM image, and (D) TEM image of Pd-ECF nanocomposites. Reprinted with permission from ref 59. (Copyright John Wiley and Sons, 2008.)

The Pd-ECF hybrids can be used directly for electrochemical sensing of H_2O_2. **Figure** 9 shows the representative current-time response of Pd-ECF//CPE at a fixed potential of 0.2 V (versus Ag/AgCl) upon successive introduction of hydrogen peroxide into nitrogen-saturated PBS (pH = 7.0) under constant stirring. It is noteworthy that the Pd-ECF//CPE sensor exhibited fast response when the analyte was introduced to the PBS solution. 95% of the steady-state current could be attained within less than five seconds.

This response time was shorter than those of sensors reported previously [67, 105, 106]. The Pd-ECF sensor exhibited a detection range from 0.2 μM to 20 mM and a sensitivity of 4.15 mA mM^{-1} (**Figure 9A, inset**). This dynamic range was broader than those of previously reported devices [107]. **Figure 9B** shows that the Pd-ECF sensor exhibited a limit of detection of 0.2 mM, which was significantly lower than those of the peroxidase-incorporated biosensors [105, 108], and Ag NP-based sensors [109]. The authors attributed the high sensitivity and broad detection range to i) the three dimensional framework composed of the Pd NP-decorated ECFs, which facilitates both ion diffusion and electron transport, and ii) the intrinsic properties of these Pd nanoparticles that result in strong electrochemical activities towards detection of hydrogen peroxide. It is worth mentioning that the Pd-ECF//CPE sensor avoids some major issues associated with H_2O_2 sensors based on peroxidases or redox mediators, such as deactivation of enzymes and leaching of mediators.

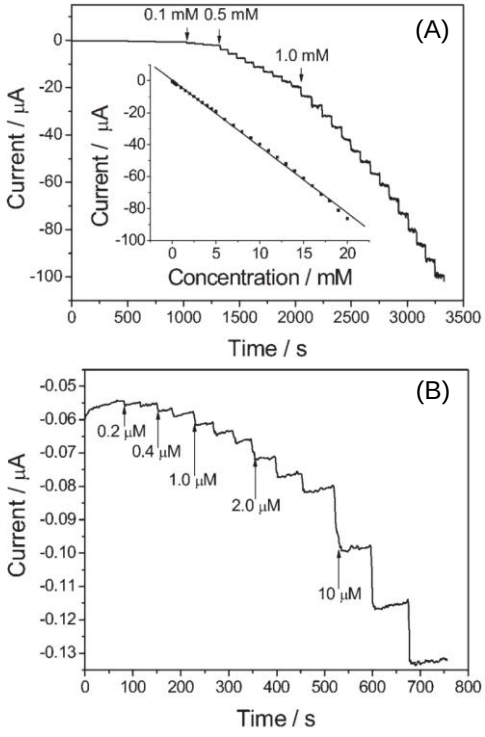

Figure 9. (A) A representative chronoamperometic profile of Pd-ECF//CPE with successive addition of different concentrations of hydrogen peroxide into N_2-saturated PBS (0.1 M, pH = 7.0). Inset: linear correlation between the current response and the H_2O_2 concentration between 0.2 μM and 20 mM. (B) The detailed current-time response of Pd-ECF//CPE at a fixed potential of 0.2 V (versus Ag/AgCl) in the presence of low concentrations of hydrogen peroxide. Reprinted with permission from ref 59. (Copyright John Wiley and Sons, 2008.)

Most recently, Lu *et al*. incorporated nickel into electrospun carbon nanofibers using a similar method as described above, where metal salts are dissolved in polymer precursors and converted to metal nanoparticles via thermal treatment. The resulting nickel-loaded carbon nanofibers are used to detect simultaneously the nucleic acids, guanine and adenine, two important components of DNA double helix [62]. Specifically, the Ni-CNF were fabricated by electrospinning a precursor mixture containing PAN/$Ni(Ac)_2$/$Zn(Ac)_2$ in DMF. Subsequent carbonization allowed the gasification of zinc oxide and resulted in a porous ECF with embedded Ni nanoparticles. The Ni-CNF was then electrochemically deposited onto a glassy carbon electrode (GCE) to serve as the sensing probe. With this electrode, guanine and adenine were detected as two well-defined and sharp oxidation peaks in 0.1 M PBS (pH 4) buffer. A linear range of 0.05 – 2 μM, with a detection limit of 0.03 μM was achieved for both guanine and adenine independently.

Procedures similar to the process discussed above to generate Pd-ECF hybrids have been used to modify electrospun carbon fibers with other metal NPs, including Ni [41, 45], Rh [44], Mn [42], and Pt [55]. These metal NP-ECF hybrid systems have been explored for the development of non-enzymatic electrochemical sensors for the detection of various important biologically relevant analytes, such as glucose, paracetamol, and H_2O_2.

In other cases, metal nanoparticle-loaded ECFs have also been combined with redox enzymes to develop enzymatic sensors. Li *et al*. reported a phenolic biosensor based on a hybrid system that consisted of polydopamine (PDA), laccase (Lac), and nickel nanoparticle-loaded carbon nanofibers (Ni-ECFs) [50]. The fabrication process for the PDA-Lac-Ni-ECF hybrid is illustrated schematically in **Figure 10**. The Ni-ECFs were shortened before mixing with other ingredients. Next a mixture of Lac and Ni-ECFs was added to a dopamine-containing acetate buffer solution (pH = 5.5) with constant stirring. Polymerization of dopamine occurred at room temperature in this mixture and the resulting polydopamine encapsulated the Lac on the surface of the Ni-ECFs. The PDA-Lac-Ni-ECF hybrid was deposited onto a magnetic glassy carbon electrode (MGCE); the PDA-Lac-Ni-ECF//MGCE was used as the sensor. As a control sample, PDA-Lac//MGCE was prepared in a similar fashion, with identical quantities of PDA and Lac.

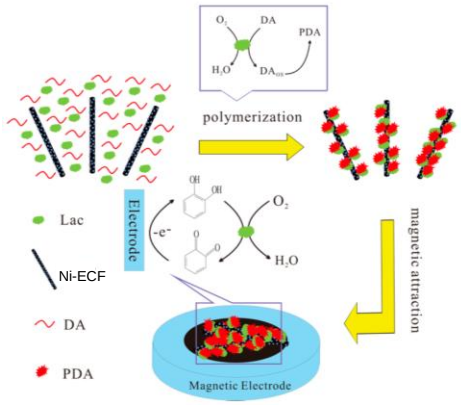

Figure 10. Schematic illustration of the fabrication processes of PDA-Lac-Ni-ECF composites and the resulting sensors. Reprinted with permission from ref 50. (Copyright American Chemical Society, 2014.)

To highlight the advantage of using Ni-ECFs, the authors compared the sensing performances of the PDA-Lac-Ni-ECFs//MGCE and PDA-Lac//MGCE using steady-

state chronoamperometry to monitor the current response when different concentrations of catechol (CC) were introduced to an acetate buffer solution (pH = 5.5) under stirring (**Figure 11A**). The enlarged image for 0 to 500 s is shown in the inset in **Figure 11A**. It can be clearly seen from **Figure 11** that in the presence of the same concentrations of CC, significantly higher currents were obtained on PDA-Lac-Ni-ECF//MGCE than on PDA-Lac//MGCE. These results indicate the important role of Ni-ECFs in the sensor to facilitate electron transfer between the substrate electrode and the analyte. **Figure 11B** shows the corresponding calibration curves for PDA-Lac-Ni-ECFs//MGCE and the PDA-Lac//MGCE; the former had a detection limit of 0.69 μM, significantly more sensitive than that of the latter (2.8 μM). PDA-Lac-Ni-ECFs//MGCE exhibited negligible current responses towards other phenolic compounds (including catechin, epicatechin, gallic acid, guaiacol, phenol, and aminophenol), indicating its excellent selectivity for catechol. In another study on the development of ECF-based enzymatic sensors [51], ECFs loaded with copper nanoparticles were mixed physically with Lac and Nafion, followed by deposition on a GCE. The resulting Cu/CNF/Lac/Nafion//GCE biosensor was used for the detection of catechol. This sensor exhibited a detection limit of 1.18 μM, lower than the value for the control system that does not contain copper nanoparticles (i.e., ECF/Lac/Nafion//GCE).

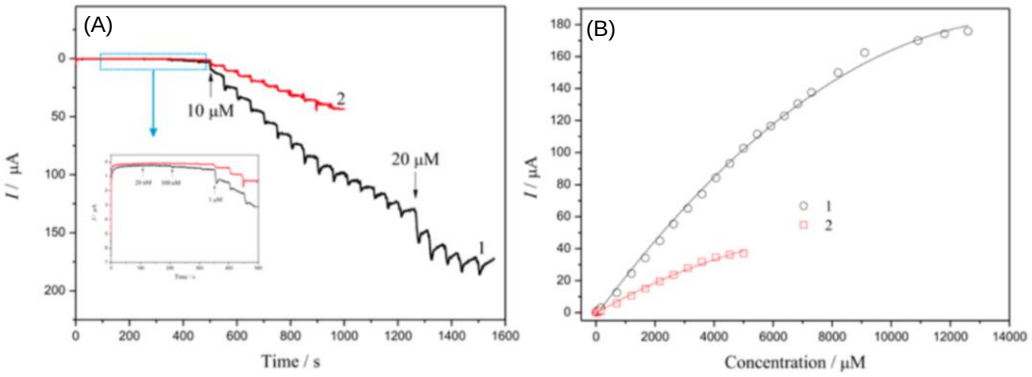

Figure 11. (A) Current-time profiles of (1) PDA-Lac-Ni-ECF//MGCE and (2) PDA-Lac//MGCE at a fixed potential of 0.4V (versus Ag/AgCl) upon successive injection of catechol solutions into an acetate buffer solution. The inset shows an enlarged image of the data in the blue rectangle. (B) The nonlinear calibration curves for (1) PDA-Lac-Ni-ECF//MGCE and (2) PDA-Lac//MGCE. Reprinted with permission from ref 50. (Copyright American Chemical Society, 2014.)

In addition to metal nanoparticles, graphene particles have been incorporated into ECFs to improve the biosensing activities of these fibers [39]. The sensor containing graphene-loaded ECFs was found to be effective in the selective detection of dopamine in the presence of uric acid and ascorbic acid. Based on square-wave voltammetry (SWV) measurements, this sensor displayed a linear dynamic range from 0.5 to 100 μM and a detection limit of 70 nM.

2.3 ECFs Post-Treated with Wet Chemical Processes

In this section, we discuss post-treatment of ECFs using wet chemical processes to introduce biosensing capabilities. These modification methods are not restricted to electrospun carbon fibers, and can be applied to other types of carbon materials such as carbon nanotubes, graphene, and CVD-grown carbon fibers.

Huang *et al*. [40] reported a seed-growth reduction process to immobilize Ag−Pt bimetallic nanoparticles onto ECFs (**Figure 12**). First, as-spun bi-component PAN/PVP fibers were extracted with water to remove the PVP component, followed by thermal treatment to carbonize the PAN component, generating porous carbon nanofibers. Second, a free-standing pristine ECF mat was immersed into a $AgNO_3$ aqueous solution, followed by reduction of Ag+ using a NaBH4 solution. Next, the Ag-ECF mat was dipped into a $H_2PtCl_6 \cdot 6H_2O$ aqueous solution to induce the partial replacement of Ag with Pt, resulting

in ECFs loaded with Ag-Pt bimetallic nanoparticles (Ag−Pt-ECFs). TEM imaging (**Figure 13**) shows that Ag−Pt bimetallic nanoparticles (also confirmed by elemental mapping) with an average size of 6 nm were uniformly distributed on the ECF surfaces. The lattice fringes with an interlayer distance of 0.23 nm (inset of **Figure 13**) correspond to the mean value of the (111) planes of the face-centered cubic Ag-Pt. Such results show that the (111) plane is the main exposed facet, and the observed nanoparticles were identified as a metal alloy of Ag and Pt atoms [110].

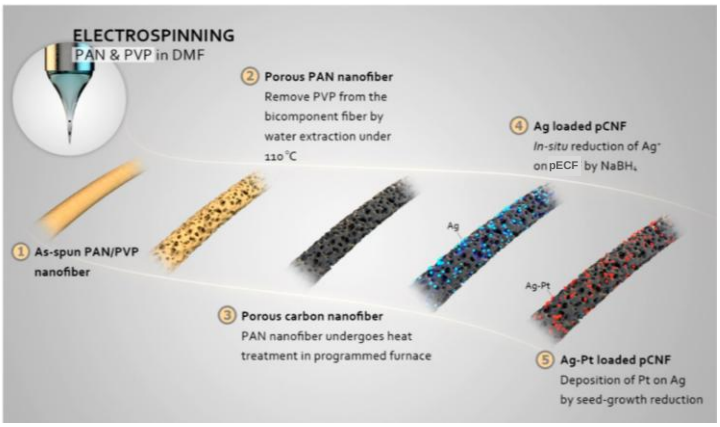

Figure 12. Schematic illustration of the preparation of Ag-Pt-ECFs. Reprinted with permission from ref 40. (Copyright American Chemical Society, 2014.)

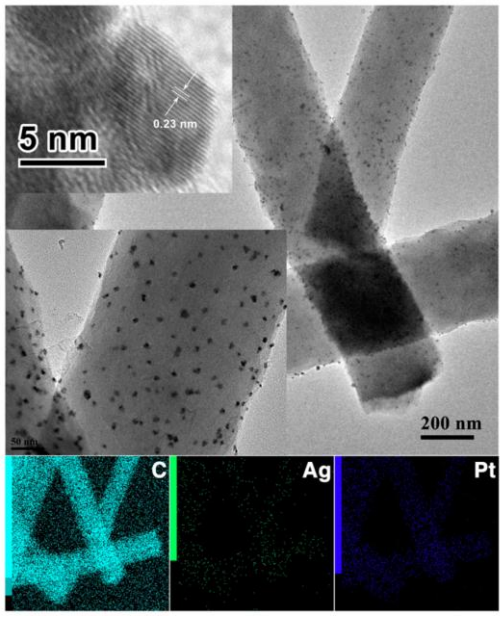

Figure 13. TEM images of Ag-Pt-ECFs and the corresponding elemental mappings. Inset: high-resolution TEM of Ag-Pt bimetallic nanoparticles. Reprinted with permission from ref 40. (Copyright American Chemical Society, 2014.)

The Ag-Pt-ECFs were then deposited onto GCE to test the electrocatalytic activities of these fibers towards dopamine. **Figure 14** shows the representative differential pulse voltammetry (DPV) curves obtained at Ag−Pt-ECFs//GCE in the presence of various concentrations of dopamine. Increasing DPV peak current with increasing dopamine concentration indicates that Ag−Pt-ECFs//GCE could be used to detect DA quantitatively. The corresponding calibration curve is shown in **Figure 14** inset, from which it can be seen that the magnitude of the peak current exhibited a linear relationship with the dopamine concentration from 10 to 500 μM. The detection limit for dopamine sensing was found to be 0.11 μM for the Ag−Pt-ECFs//GCE sensor.

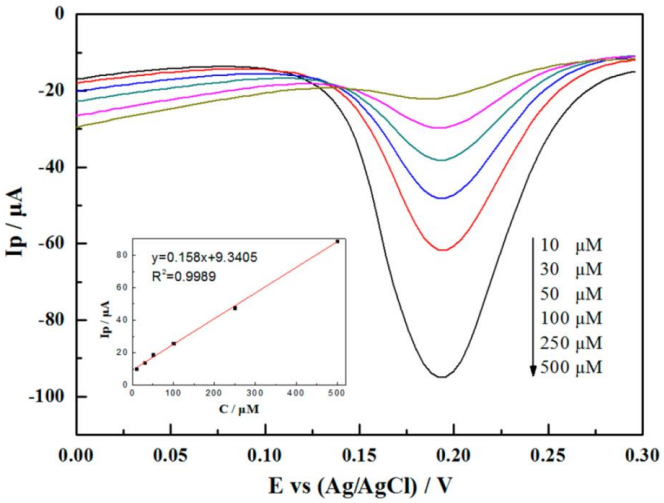

Figure 14. Differential pulse voltammetric profiles of Ag-Pt-pECFs//GCE in the presence of different dopamine concentrations in nitrogen-saturated PBS. From top to bottom, the dopamine concentration is 10, 30, 50, 100, 250, 500 μM. Inset: the linear calibration curve. Reprinted with permission from ref 40. (Copyright American Chemical Society, 2014.)

In another study, a controllable wet-chemical method was used for post-modification of as-synthesized ECFs to fabricate Pt nanoparticle-loaded carbon fibers for H_2O_2 sensing applications [57]. Without any pretreatment, the as-carbonized fibers could be easily modified with Pt nanoparticles by immersing the ECFs into a H_2PtCl_6 solution followed by reduction using HCOOH. In this modification process, the H_2PtCl_6 concentration had a remarkable effect on the morphologies of the Pt-ECF hybrids. The SEM images of Pt-ECF hybrids prepared using solutions with different H_2PtCl_6 concentrations are shown in **Figure 15**. With 1 mM H_2PtCl_6, a uniform distribution of Pt nanoparticles on the carbon fiber surface without aggregation was attained. When the concentration was at 2 mM, a complete surface coverage of Pt was achieved, but at the expense of a possible weakening of the anti-fouling properties attributed to the carbon surfaces. Several species in the "real world" samples, such as chloride anions, amino acids, and proteins, are known to adhere strongly to the electrode surface, particularly the surface of platinum. Severe electrode fouling can render the surface inaccessible to the target analyte. Carbon surfaces are usually resistant to surface fouling. When using a very high H_2PtCl_6 concentration (3 mM), large chunks of Pt particles with irregular shapes were formed, possibly leading to low catalytic efficiencies and poor reproducibility in terms of the sensing performance. Therefore, 1 mM was proposed to be the optimal concentration for modification of ECFs with Pt nanoparticles. The steady-state amperometric response of the Pt-ECF sensor to successive injections of H_2O_2 is shown in **Figure 16**. It is evident that the sensor displayed rapid responses to different concentrations of H_2O_2 from 1 to 800 μM; the detection limit was found to be 0.6 μM.

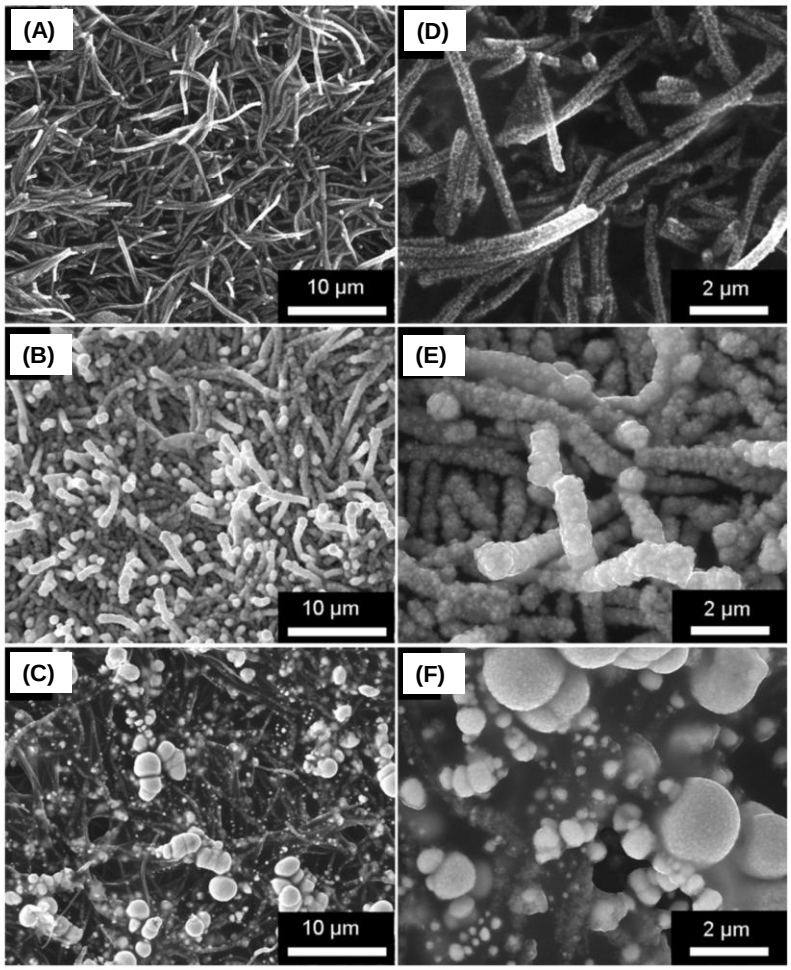

Figure 15. SEM images of the Pt-ECF electrodes prepared from a precursor solution that contains H_2PtCl_6 with the concentration of (A) 1 mM, (B) 2 mM and (C) 3 mM. Panels (D), (E) and (F) are the enlarged SEM images of panels (A), (B) and (C), respectively. Reprinted with permission from ref 57. (Copyright Elsevier, 2011.)

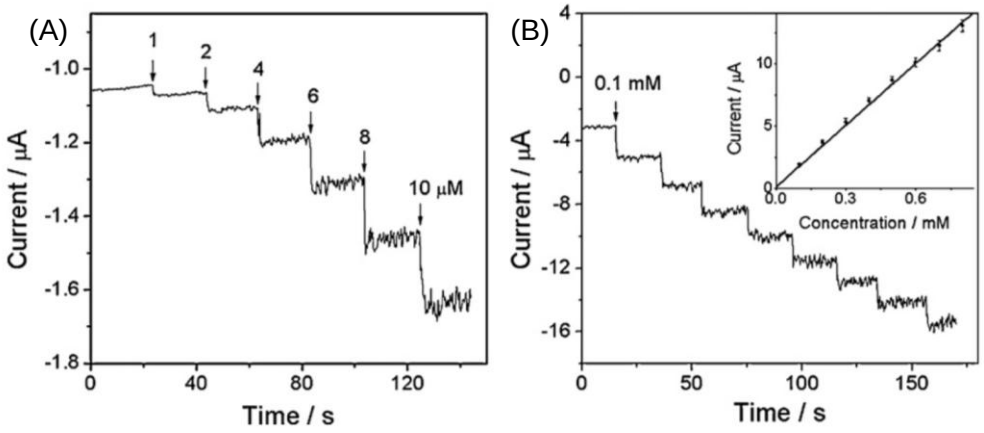

Figure 16. A representative chronoamperometric profile of the Pt-ECF electrode at a fixed potential of 0 V (versus Ag/AgCl) with successive injection of hydrogen peroxide at (A) low concentrations and (B) 0.1 mM. Inset of (B) shows the linear relationship between the current and the H_2O_2 concentration. Reprinted with permission from ref 57. (Copyright Elsevier, 2011.)

Lin *et al.* reported a method to prepare Pd nanoparticle-loaded ECFs by electrodeposition of Pd onto electrospun carbon fibers, for use as sensing materials for detection of H_2O_2 and NADH [58]. The TEM images of the as-prepared ECFs and Pd-ECF hybrids are shown in **Figure 17A, B**. The ECFs without modification showed smooth surfaces, while the Pd-ECF hybrids exhibited interesting dendritic Pd structures, which were also observed by SEM (**Figure 17C**). A possible growth mechanism of the dendritic Pd structures on the carbon fiber surface is illustrated schematically in **Figure 18.** In the initial stage, Pd nuclei on the fiber surface were generated through the electroreduction process by application of a negative potential to the carbon fiber electrode (**Figure 18A**), followed by the growth of the nuclei to supercritical clusters (**Figure 18B**). With increasing electrodeposition time, Pd clusters grew along the <111> direction (**Figure 18C**), mainly because SO_4^{2-}, which was present in the deposition solution, preferentially adsorbed on the Pd (111) surfaces, disturbing their growth in the direction that is normal to the (111) plane [111, 112]. Such preferential adsorption of SO_4^{2-} on the (111) surface of a metal has also been observed with a Pt (111) electrode [113]. It was found that the ECFs with the dendritic Pd clusters exhibited higher current responses towards H_2O_2 and NADH than did the ECFs with spherical Pd particles, although the sensing performances of these Pd-ECF sensors, such as the detection limit and the dynamic range, were not investigated in this study.

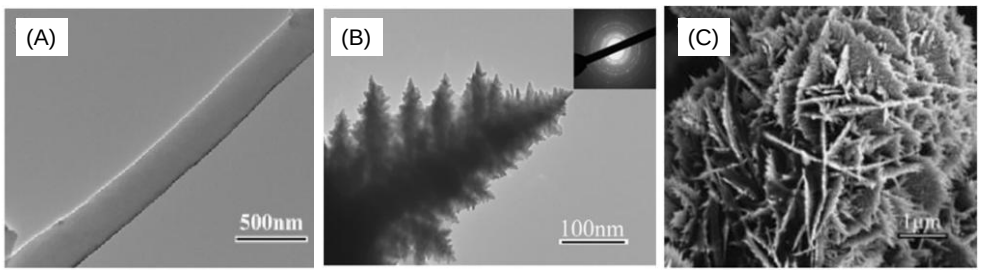

Figure 17. TEM images of (A) ECF and (B) Pd-ECF. The inset in (B) shows the electron diffraction pattern of the TEM image. (C) SEM image of Pd-ECF prepared from a deposition potential of −0.2 V (versus Ag/AgCl) and a deposition time of 4 h. Reprinted with permission from ref 58. (Copyright Springer, 2011.)

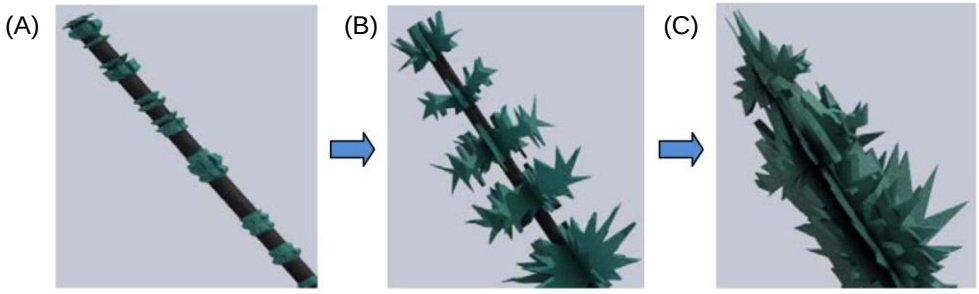

Figure 18. Schematic illustration of a possible growth mechanism of dendritic Pd structures on an ECF. (A) Formation of seeding nuclei. (B) Supercritical cluster formation. (C) Generation of dendritic structures. Reprinted with permission from ref 58. (Copyright Springer, 2011.)

3. Summary

Electrospun carbon fibers represent a class of one-dimensional meso- or nano-structured carbon materials that can be prepared by a facile and flexible process consisting of electrospinning of precursor solutions and subsequent carbonization. The development of ECF-based electrochemical sensors with high sensitivities, high selectivity, and wide detection ranges is of importance in both chemical and biological industries for a variety of applications such as water treatment, clinical chemistry and bioprocessing.

Manipulation of carbonization conditions is the main strategy to improve sensing capabilities of ECFs. This strategy consists of the fewest number of processing steps and requires no additional functional components such as metal nanoparticles. An understanding of the relationship between carbon microstructures and thermal treatment conditions is necessary for the development of sensors using this method. However the sensing capabilities introduced here are limited by the intrinsic properties of carbon materials. As a result, analytes that respond only to non-carbon components (e.g., gold nanoparticles, enzymes) cannot be detected using sensors fabricated by this strategy. Another important method to impart sensing functionalities into ECFs is through incorporation of metal nanoparticles by variation of the composition of the precursor solution. This method makes use of the electrochemical activities of the metallic components, thereby providing sensing capabilities for certain analytes that cannot be detected directly by carbon-based sensors alone. On the other hand, the increased cost due to the use of metals such as Pt is a disadvantage of this method. Another strategy to develop ECF sensors is through post-functionalization of as-synthesized ECFs with electroactive components. Such functionalization is usually achieved by wet chemical processes, which are flexible enough to create, for instance, metal nanoparticles with complicated morphologies and chemical compositions (e.g., synthesis of bimetallic particles, generation of dendritic metal structures). These types of electroactive components are difficult to fabricate by control over the composition of the precursor solution. However, the post-treatment procedures usually require that the as-spun ECFs be milled to break up the fibers, which may compromise the electron transfer properties relative to those of continuous carbon fibers. Modifications strategies such as control

over thermal treatment conditions and post-treatment by wet chemical processes can also be applied to other types of carbon materials such as carbon nanotubes and graphene. However, variation of the composition of the precursor solution prior to electrospinning is a method that works almost exclusively for ECFs. Compared to CNT- or graphene-based sensing materials, ECFs with electrochemical activities introduced by the three structural modulation strategies discussed above enjoy several advantages, such as ease of fabrication, controllable morphology and porosity by changing the electrospinning conditions and, in the cases of integrated fiber mats, good electron transport properties due to the continuous nature of ECFs.

ECF-based sensing devices are prepared by either drop-casting of fiber-containing suspensions onto substrates, or through the use of free-standing fiber mats. Generally, sensors prepared by the first method exhibit a lower background current, a higher sensitivity and better fabrication reproducibility, while sensors fabricated by the second approach usually have larger electroactive surface areas and thus afford a wider detection range, but also show poor fabrication reproducibility. One strategy to combine the advantages from both types of methods is to electrospin polymer fibers directly onto a conductive substrate followed by carbonization of the substrate/fiber assembly, generating substrate-supported continuous fibers. Electrochemical sensors prepared *via* this route have been shown to display a high sensitivity, a wide detection range, and good fabrication reproducibility [53].

ECF-based sensors have been used for detection of a range of biologically relevant molecular systems, including ascorbic acid, maltose, glucose, fructose, catechol, dopamine, paracetamol, formaldehyde, L-cysteine, sucrose, hydrazine, L-tyrosine, uric

acid, hydrogen peroxide, hydroquinone, L-tryptophan, and xanthine. The general principles for improving the electrochemical biosensing performance of ECF-based material systems include (i) control over the intrinsic electronic properties of polymer-derived carbon materials such as valence and conduction band structures, and (ii) addition of non-carbon functional ingredients that display electrochemical activities and selectivity towards specific types of analytes.

ECFs have been used for the development of both enzymatic and non-enzymatic sensors. For certain types of analytes such as H_2O_2 and glucose, the carbon fibers usually do not display any electrochemical activity, and thus incorporation of enzymes having catalytic activity towards these molecules is necessary. In these cases, the role of the carbon fiber is to serve as a conductive substrate for transferring electrons to the redox-active enzymes. Additionally, the porous structures resulting from the fiber assemblies are conducive to accommodation of enzymes. The electron transfer efficiencies between ECFs and enzymes can be enhanced by modulation of the electronic structure of the carbon fibers, particularly the DOS at the Fermi level, through control of the carbonization conditions when treating as-spun polymer fibers. Metal nanoparticle-loaded ECFs can usually function as non-enzymatic sensors since the metallic components usually exhibit very high electrocatalytic activities for a range of redox molecules that cannot be detected by the carbon component alone. Compared to enzymatic sensors, non-enzymatic sensors enjoy advantages such as high stability and low cost.

ECFs can potentially be used as immobilization matrices for biorecognition agents to detect antibodies, antigens and DNAs. Based on highly specific interactions

between sensors and analytes, immunosensors and DNA hybridization sensors are especially attractive; these sensors can be assembled by incorporating biorecognition agents into carbon nanofibers, with which to bind certain analytes selectively, such as antibodies and receptors for nucleic acids, or oligonucleotides. The molecular recognition of those sensors solely relies on the complementary size and shape of the binding site to the analyte. The inherent specificity of biorecognition agents to the target analytes often results in excellent selectivity for detecting individual analytes in a mixture [114]. Carbon nanofibers produced by methods other than electrospinning have been used as immobilization matrixes for antigens or antibodies due to their excellent electron transfer kinetics, biocompatibility [76], large surface area, high concentration of surface active groups, and abundance of edge-plane sites [115]. Recently, a carbon nanofiber-based immunosensor for recombinant bovine somatotropin was developed by site-directed immobilization of antibodies onto commercial screen-printed carbon nanofiber electrodes that were fabricated via chemical vapor deposition [116]. A detection limit of 1 pg/mL with a linear dynamic range of 1 pg/mL to 10 ng/mL was achieved. To the best of our knowledge, carbon nanofibers that were fabricated via electrospinning have not been reported for immunosensor or DNA sensor applications. However, electrospun carbon nanofibers can potentially be easily incorporated as the immobilization matrix, which may allow further optimizations and developments that are enabled by the versatility of the electrospinning technique and carbonization process.

4 Outlook

While significant progress on ECF-based sensing materials has been achieved, there is still significant room for a detailed study into the fundamentals of ECF electrochemistry, and additional challenges must be addressed before ECF-based devices can be fully commercialized. Modeling of the electrochemistry of carbon based on its electronic structures is important for a fundamental understanding of the performance of carbon-based sensors. For ECF systems, PAN is the most commonly used precursor; carbonization of PAN at temperatures of 700 to 1500 °C results in turbostratic, defect-rich carbon structures, and the choice of the carbonization temperature has a significant impact on the electronic structure of the carbon fibers. One of the most important factors governing the heterogeneous electron transfer (HET) activities of an electrode material is its electronic structure; the efficiencies of electron exchange at an electrode/electrolyte interface depend strongly on the overlap between the energy levels of the electrode material and the redox states in solution [1, 117, 118]. However, quantitative relationships between the electronic structure of ECFs and their electrochemical activity are rarely presented. The electrochemistry of ECFs with tunable electronic properties can be modeled by the Gerischer-Marcus (GM) theory [119-121], which provides a quantitative description of the DOS dependence of electrode kinetics. According to the GM formulism, HET on ECFs is not restricted to the Fermi levels of the interacting species only, but rather is dictated by the DOS of the carbon fibers and the distribution of the redox states in the solution phase. More specifically, the HET rate constant can be specified quantitatively based on the overlap of the valence band (or conduction band) DOS of the carbon fiber and the distribution of the unoccupied (or occupied) redox states in solution [119-121]. Also, such a model can be used to delineate the relationship

between the electron transfer rate and the overpotential, which may provide valuable insights into the detailed electronic properties of the electrode systems, such as the fingerprints of the distinct van Hove singularities for single-walled carbon nanotubes [26, 121]. Furthermore, theoretical models that relate selectivity of carbon electrodes to their electronic properties are scarce, and progress in this direction is desired, to establish general design principles and develop useful descriptors for carbon-based electrochemical biosensing materials.

A second area for further investigation is the role of the synergistic effects between the carbon and non-carbon components. It has been found that significant chemical coupling between inorganic nanoparticles and carbon nanotubes or graphene resulted in modulation of the electronic properties of each individual component; such modulation serves to provide the resulting hybrid systems with strong electrochemical activities toward oxygen reduction reactions (ORRs) [108, 109, 114]. For example, CoO-carbon nanotube hybrids [122] and CoO-graphene [123] have been reported to function as effective electrocatalysts for ORR. Perturbation of the electronic structure of electrode materials should change their electrochemical activity towards redox-active molecules, as predicted by electron transfer theory. There it can be expected that the coupling effects between ECFs and various metal nanoparticles should play an important role in the sensing performance in the resulting hybrids. The coupling effects could be elucidated by evaluation of the variation in electronic structure before and after modification of carbon fibers with other non-carbon functional ingredients, using spectroscopic techniques such as UPS, EELS, carbon K-edge and metal L-edge XANES. In principle, modification strategies that influence electronic structure of ECFs are expected to affect their sensing

performance. To date, the modification methods that have been applied to ECFs are limited to variations in carbonization conditions and incorporation of metal nanoparticles. It is of interest to study other methods that perturb the carbon electronic structure, such as doping with heteroatoms, controlled oxidation, and adsorption of polyelectrolytes or surfactants.

Due to the surface heterogeneity of ECFs, special emphasis should be placed on the interpretation of the electron transfer kinetics obtained on these fibers. In most cases, the surfaces of ECFs consist of areas of different electrochemical activity, such as edge defects versus basal planes, and carbon supports versus metal nanoparticles. Use of advanced *in situ* surface characterization methods such as electrochemical microscopy and spectroscopy with spatial resolution may be helpful for detailed examination of the dependence of electron transfer processes on the surface heterogeneity.

In addition to the aforementioned aspects related to the fundamentals of ECF electrochemistry, there are also several challenges regarding the practical applications of ECF-sensing devices that must be addressed. First, the scale-up ability and cost-effectiveness of the ECF production and sensor fabrication processes should be considered. Recently, free surface or "needle-less" electrospinning [34] has been reported to be able to generate high-quality fiber mats with good reproducibility and high productivity. However, for producing metal nanoparticle-decorated fibers that have proven useful for electrochemical detection of various biologically relevant molecules, complicated customized multi-fluidic nozzles or multi-step post-treatment procedures are necessary, which increases the complexity and cost of mass manufacturing. Second, long-term stability is an important factor in the overall performance of electrochemical sensors.

For cases where metal nanoparticles contribute dominantly to the sensing performance, electrochemical stability of these metallic components should be evaluated. For enzymatic sensors, preservation of the bioactivity of enzymes immobilized on ECFs is a prerequisite for practical applications, and thus should be studied. Additionally, the anti-fouling properties of electrochemical sensors are a major concern for use in testing with "real world" samples. Although carbon fibers are usually resistant to surface fouling, incorporation of electroactive metal species such as Pt nanoparticles may reduce this resistance. Many species that are present in the real world samples, such as chloride anions, amino acids, and proteins are known to adhere strongly to the surface of platinum. Moreover, the heterogeneous electron transfer kinetics on carbon surface are affected significantly by inadvertent adsorption of contaminants. Therefore, for ECF systems, particularly those decorated with metal nanoparticles, evaluation of the tolerance to electrode fouling is recommended. Unfortunately, the sensing performances of ECF-based devices are rarely evaluated with respect to "real world" samples. To demonstrate utility, the reported detection limit should be compared to the common concentration ranges of analytes in practical applications. For example, 0.04 μg-equivalents/ml of hydroquinone has been reported to be safe for daily human intake [124]. Meanwhile, hydroquinone has been found at 0.2 ppm in coffee, 0.5 ppm in red wine, 0.2-0.4 ppm in wheat cereals, and 0.1 ppm in broccoli [125]. The plasma reference concentration of dopamine in supine adults is less than 10 ng/mL (0.065 nmol/L) [126]. The therapeutic dose of acetaminophen in serum is 5 to 20 mg/L, but approaches toxic levels already when the concentration is higher than 25-150 mg/L. The glucose concentration in human tears is around 5-148 μM [127]. For fertility testing, the normal concentration of fructose

in semen is 13 μM [128]. According to the US Environmental Protection Agency, the low threshold limit value of hydrazine, a probable human carcinogen, is 10 ppb [129]. To compete successfully with other existing devices at these levels, improvements in the sensing performance of ECF-based devices are still needed; CNT- or graphene-based biosensors [130-147] have already been shown to exhibit lower detection limits for various redox systems than those for ECF sensors (**Figure 19**). The excellent performance and established design principles of CNT- and graphene-based sensors are mainly attributed to (i) the high consistency and reproducibility in the fabrication of CNTs and graphene-based sensing materials, and (ii) strong correlation between the electronic structures of nanotubes and graphene and their electrochemistry. For ECF sensors, the issue of high LODs generally arises from the large background currents and inconsistency in device fabrication. Therefore, to increase the competitiveness of ECF-based devices, special attention should be paid to the device-to-device variability, careful evaluation of the microstructural and electronic properties, and minimization of background currents through control of surface chemistry/structures and fiber load masses.

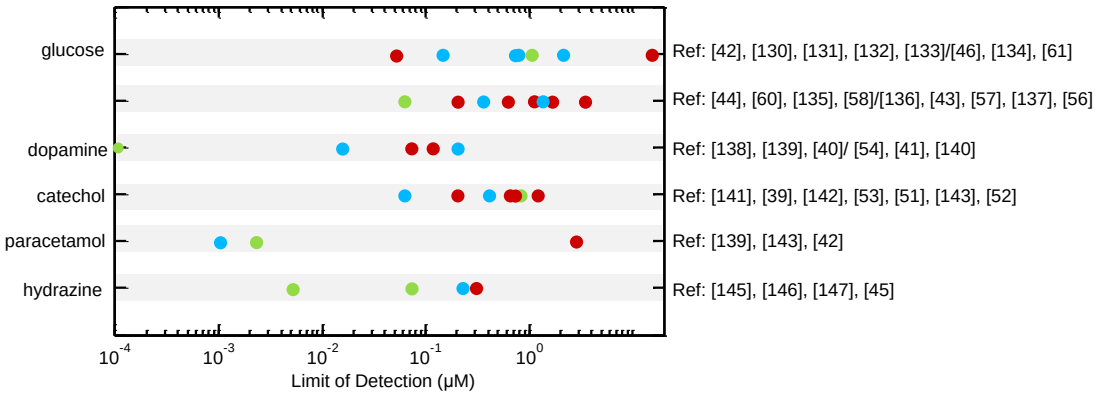

Figure 19. Comparison of LODs of ECF-based sensors (red) with those of CNT (blue) - and graphene (green) - based electrochemical sensors for various analytes. The references

corresponding to the data are listed on the left. The references of overlapped data points are separated by a forward slash.

Acknowledgements

X.M. acknowledges financial support by a Skoltech Fellowship during the preparation of this review.

Conflict of Interest

The authors declare no conflict of interest.

References

1. McCreery RL (2008) Chem Rev 108: p. 2646-2687
2. Ambrosi A, Chua CK, Bonanni A, and Pumera M (2014) Chem Rev 114: p. 7150-7188
3. Mao X, Rutledge GC, and Hatton TA (2014) Nano Today 9: p. 405-432
4. Buriak JM (2001) Angew Chem Int Edit 40: p. 532-534
5. Pinson J and Podvorica F (2005) Chem Soc Rev 34: p. 429-439
6. Mao X, Rutledge GC, and Hatton TA (2013) Langmuir 29: p. 9626-34
7. Mao X, Simeon F, Achilleos DS, Rutledge GC, and Hatton TA (2013) J Mater Chem A 1: p. 13120-13127
8. Sgobba V, Rahman GMA, Guldi DM, Jux N, Campidelli S, and Prato M (2006) Adv Mater 18: p. 2264-2269
9. Ehli C, Rahman GMA, Jux N, Balbinot D, Guldi DM, Paolucci F, Marcaccio M, Paolucci D, Melle-Franco M, Zerbetto F, Campidelli S, and Prato M (2006) J Am Chem Soc 128: p. 11222-11231
10. Guldi DM, Rahman GMA, Prato M, Jux N, Qin SH, and Ford W (2005) Angew Chem Int Edit 44: p. 2015-2018
11. Peng X, Komatsu N, Bhattacharya S, Shimawaki T, Aonuma S, Kimura T, and Osuka A (2007) Nat Nanotechnol 2: p. 361-365
12. Cheng FY, Zhang S, Adronov A, Echegoyen L, and Diederich F (2006) Chem-Eur J 12: p. 6062-6070
13. Guldi DM, Taieb H, Rahman GMA, Tagmatarchis N, and Prato M (2005) Adv Mater 17: p. 871-875
14. Mao X, Tian W, Wu J, Rutledge GC, and Hatton TA (2015) J Am Chem Soc 137: p. 1348-1355
15. Tian W, Mao X, Brown P, Rutledge GC, and Hatton TA (2015) Adv Funct Mater 25: p. 4803-4813
16. Bacon R (1960) J Appl Phys 31: p. 283-290
17. Pierson HO (1993) Handbook of carbon, graphite, diamond and fullerenes. Noyes Publications, New Jersey
18. Inagaki M, Yang Y, and Kang FY (2012) Adv Mater 24: p. 2547-2566
19. Theron SA, Zussman E, and Yarin AL (2004) Polymer 45: p. 2017-2030

20. Bhardwaj N and Kundu SC (2010) Biotechnol Adv 28: p. 325-347
21. Teo WE and Ramakrishna S (2006) Nanotechnology 17: p. 89-106
22. Sun ZC, Zussman E, Yarin AL, Wendorff JH, and Greiner A (2003) Adv Mater 15: p. 1929-1932
23. McCann JT, Li D, and Xia YN (2005) J Mater Chem 15: p. 735-738
24. Zhao Y, Cao XY, and Jiang L (2007) J Am Chem Soc 129: p. 764-765
25. Mao X, Hatton TA, and Rutledge GC (2013) Curr Org Chem 17: p. 1390-1401
26. Dumitrescu I, Unwin PR, and Macpherson JV (2009) Chem Commun: p. 6886-6901
27. Vashist SK, Zheng D, Al-Rubeaan K, Luong JHT, and Sheu FS (2011) Biotechnol Adv 29: p. 169-188
28. Chen D, Tang LH, and Li JH (2010) Chem Soc Rev 39: p. 3157-3180
29. Walker PL, Thrower, PA (1973) Chemistry and physics of carbon. Dekker, New York
30. Kinoshita K (1988) Carbon: Electrochemical and physicochemical properties. John Wiley and Sons, New York
31. McCreery RL (1991) Electroanalytical chemistry. Dekker, New York
32. Rutledge GC and Fridrikh SV (2007) Adv Drug Deliver Rev 59: p. 1384-1391
33. Forward KM and Rutledge GC (2012) Chem Eng J 183: p. 492-503
34. Forward KM, Flores A, and Rutledge GC (2013) Chem Eng Sci 104: p. 250-259
35. Shuakat MN and Lin T (2014) J Nanosci Nanotechno 14: p. 1389-1408
36. Xie K, Qin XT, Wang XZ, Wang YN, Tao HS, Wu Q, Yang LJ, and Hu Z (2012) Adv Mater 24: p. 347-352
37. Mao X, Yang X, Wu J, Tian W, Rutledge GC, and Hatton TA (2015) Chem Mater 27: p. 4574-4585
38. Guo QH, Huang JS, Chen PQ, Liu Y, Hou HQ, and You TY (2012) Sensor Actuat B-Chem 163: p. 179-185
39. Ekabutr P, Sangsanoh P, Rattanarat P, Monroe CW, Chailapakul O, and Supaphol P (2014) J Appl Polym Sci 131: p. 40858-40867
40. Huang YP, Miao YE, Ji SS, Tjiu WW, and Liu TX (2014) ACS Appl Mater Inter 6: p. 12449-12456
41. Li LL, Zhou TT, Sun GY, Li ZH, Yang WX, Jia JB, and Yang GC (2015) Electrochim Acta 152: p. 31-37
42. Xiao XP, Song YH, Liu HY, Xie MY, Hou HQ, Wang L, and Li Z (2013) J Mater Sci 48: p. 4843-4850
43. Maji SK, Sreejith S, Mandal AK, Ma X, and Zhao YL (2014) ACS Appl Mater Inter 6: p. 13648-13656
44. Hu GZ, Zhou ZP, Guo Y, Hou HQ, and Shao SJ (2010) Electrochem Commun 12: p. 422-426
45. Liu Y, Teng H, Hou HQ, and You TY (2009) Biosens Bioelectron 24: p. 3329-3334
46. Kimmel DW, LeBlanc G, Meschievitz ME, and Cliffel DE (2012) Anal Chem 84: p. 685-707
47. Liu YX, Dong XC, and Chen P (2012) Chem Soc Rev 41: p. 2283-2307
48. Gupta VK, Jain R, Radhapyari K, Jadon N, and Agarwal S (2011) Anal Biochem 408: p. 179-196

49. Alghamdi AH (2010) Arab J Chem 3: p. 1-7
50. Li DW, Luo L, Pang ZY, Ding L, Wang QQ, Ke HZ, Huang FL, and Wei QF (2014) ACS Appl Mater Inter 6: p. 5144-5151
51. Fu JP, Qiao H, Li DW, Luo L, Chen K, and Wei QF (2014) Sensors-Basel 14: p. 3543-3556
52. Li DW, Pang ZY, Chen XD, Luo L, Cai YB, and Wei QF (2014) Beilstein J Nanotech 5: p. 346-354
53. Mao X, Yang X, Rutledge GC, and Hatton TA (2014) ACS Appl Mater Inter 6: p. 3394-3405
54. Liu Y, Wang DW, Huang JS, Hou HQ, and You TY (2010) Electrochem Commun 12: p. 1108-1111
55. Yang Y, Fu RZ, Wang HY, and Wang C (2013) Microchim Acta 180: p. 1249-1255
56. Mao X, Simeon F, Rutledge GC, and Hatton TA (2013) Adv Mater 25: p. 1309-1314
57. Liu Y, Wang DW, Xu L, Hou HQ, and You TY (2011) Biosens Bioelectron 26: p. 4585-4590
58. Lin Z, Ji LW, Medford AJ, Shi Q, Krause WE, and Zhang XW (2011) J Solid State Electr 15: p. 1287-1294
59. Huang JS, Wang DW, Hou HQ, and You TY (2008) Adv Funct Mater 18: p. 441-448
60. Liu D, Zhang XP, and You TY (2014) ACS Appl Mater Inter 6: p. 6275-6280
61. Tang XF, Liu Y, Hou HQ, and You TY (2011) Talanta 83: p. 1410-1414
62. Lu YL, Luo LQ, Ding YP, Wang YH, Zhou M, Zhou TY, Zhu D, and Li XY (2015) Electrochim Acta 174: p. 191-198
63. Pimenta MA, Dresselhaus G, Dresselhaus MS, Cancado LG, Jorio A, and Saito R (2007) Phys Chem Chem Phys 9: p. 1276-1291
64. Wiggins-Camacho JD and Stevenson KJ (2009) J Phys Chem C 113: p. 19082-19090
65. Cuomo JJ, Doyle JP, Bruley J, and Liu JC (1991) 58: p. 466-468
66. Ueda A, Kato D, Kurita R, Kamata T, Inokuchi H, Umemura S, Hirono S, and Niwa O (2011) J Am Chem Soc 133: p. 4840-4846
67. Liu Y, Qu XH, Guo HW, Chen HJ, Liu BF, and Dong SJ (2006) Biosens Bioelectron 21: p. 2195-2201
68. Kamin RA and Wilson GS (1980) Anal Chem 52: p. 1198-1205
69. Maldonado S and Stevenson KJ (2005) J Phys Chem B 109: p. 4707-4716
70. Reneker DH and Chun I (1996) Nanotechnology 7: p. 216-223
71. Qiu Y, Yu J, Shi T, Zhou X, Bai X, and Huang JY (2011) J Power Sources 196: p. 9862-9867
72. Pels JR, Kapteijn F, Moulijn JA, Zhu Q, and Thomas KM (1995) Carbon 33: p. 1641-1653
73. Strelko VV, Kuts VS, and Thrower PA (2000) Carbon 38: p. 1499-1503
74. Qureshi A, Kang WP, Davidson JL, and Gurbuz Y (2009) Diam Relat Mater 18: p. 1401-1420
75. Ndamanisha JC and Guo LP (2012) Anal Chim Acta 747: p. 19-28
76. Jacobs CB, Peairs MJ, and Venton BJ (2010) Anal Chim Acta 662: p. 105-127

77. Kuila T, Bose S, Khanra P, Mishra AK, Kim NH, and Lee JH (2011) Biosens Bioelectron 26: p. 4637-4648
78. Zhang MN, Yu P, and Mao LQ (2012) Accounts Chem Res 45: p. 533-543
79. Wilson GS and Gifford R (2005) Biosens Bioelectron 20: p. 2388-2403
80. Zhou M and Dong SJ (2011) Accounts Chem Res 44: p. 1232-1243
81. Kim C, Yang KS, Kojima M, Yoshida K, Kim YJ, Kim YA, and Endo M (2006) Adv Funct Mater 16: p. 2393-2397
82. Cao XH, Zhang LX, Cai WP, and Li YQ (2010) Electrochem Commun 12: p. 540-543
83. Min K and Yoo YJ (2009) Talanta 80: p. 1007-1011
84. Zheng D, Ye JS, and Zhang WD (2008) Electroanal 20: p. 1811-1818
85. Li YX, Wang P, Wang L, and Lin XQ (2007) Biosens Bioelectron 22: p. 3120-3125
86. Shahrokhian S and Zare-Mehrjardi HR (2007) Electrochim Acta 52: p. 6310-6317
87. Yogeswaran U and Chen SM (2008) Sensor Actuat B-Chem 130: p. 739-749
88. Zhang YZ, Pan Y, Sit S, Zhang LP, Li SP, and Shao MW (2007) Electroanal 19: p. 1695-1701
89. Kan XW, Zhao Y, Geng ZR, Wang ZL, and Zhu JJ (2008) J Phys Chem C 112: p. 4849-4854
90. Xiang L, Lin YQ, Yu P, Su L, and Mao LQ (2007) Electrochim Acta 52: p. 4144-4152
91. Tsai YC and Chiu CC (2007) Sensor Actuat B-Chem 125: p. 10-16
92. Manjunatha R, Suresh GS, Melo JS, D'Souza SF, and Venkatesha TV (2010) Sensor Actuat B-Chem 145: p. 643-650
93. Alothman ZA, Bukhari N, Wabaidur SM, and Haider S (2010) Sensor Actuat B-Chem 146: p. 314-320
94. Kim YR, Bong S, Kang YJ, Yang Y, Mahajan RK, Kim JS, and Kim H (2010) Biosens Bioelectron 25: p. 2366-2369
95. Liu SQ, Sun WH, and Hu FT (2012) Sensor Actuat B-Chem 173: p. 497-504
96. Liu X, Xie LL, and Li HL (2012) J Electroanal Chem 682: p. 158-163
97. Liu Q, Zhu X, Huo ZH, He XL, Liang Y, and Xu MT (2012) Talanta 97: p. 557-562
98. Sun CL, Chang CT, Lee HH, Zhou JG, Wang J, Sham TK, and Pong WF (2011) ACS Nano 5: p. 7788-7795
99. Han DX, Han TT, Shan CS, Ivaska A, and Niu L (2010) Electroanal 22: p. 2001-2008
100. Zhang Y, Yuan R, Chai YQ, Li WJ, Zhong X, and Zhong HA (2011) Biosens Bioelectron 26: p. 3977-3980
101. Van der Lee MK, Van Dillen AJ, Bitter JH, and De Jong KP (2005) J Am Chem Soc 127: p. 13573-13582
102. Qiu JS, Zhang HZ, Liang CH, Li JW, and Zhao ZB (2006) Chem-Eur J 12: p. 2147-2151
103. Tian ZQ, Jiang SP, Liang YM, and Shen PK (2006) J Phys Chem B 110: p. 5343-5350
104. Sevilla M and Fuertes AB (2006) Carbon 44: p. 468-474
105. Lei CH and Deng JQ (1996) Anal Chem 68: p. 3344-3349

106. Huang WM, Jia JB, Zhang ZL, Han XJ, Tang JL, Wang JG, Dong SJ, and Wang EK (2003) Biosens Bioelectron 18: p. 1225-1230
107. Wu S, Zhao H, Ju H, Shi C, and Zhao J (2006) Electrochem Commun 8: p. 1197-1203
108. Jia JB, Wang BQ, Wu AG, Cheng GJ, Li Z, and Dong SJ (2002) Anal Chem 74: p. 2217-2223
109. Welch CM, Banks CE, Simm AO, and Compton RG (2005) Anal Bioanal Chem 382: p. 12-21
110. Chai J, Li F, Hu Y, Zhang Q, Han D, and Niu L (2011) J Mater Chem 21: p. 17922-17929
111. Hoshi N, Kuroda M, Koga O, and Hori Y (2002) J Phys Chem B 106: p. 9107-9113
112. Nakamura M, Sakurai Y, and Ito M (2004) J Electroanal Chem 563: p. 63-69
113. Kolics A and Wieckowski A (2001) J Phys Chem B 105: p. 2588-2595
114. Ronkainen NJ, Halsall HB, and Heineman WR (2010) Chem Soc Rev 39: p. 1747-1763
115. Huang JS, Liu Y, and You TY (2010) Anal Methods-Uk 2: p. 202-211
116. Lim SA and Ahmed MU (2015) Biosens Bioelectron 70: p. 48-53
117. Chen S, Liu Y, and Chen J (2014) Chem Soc Rev 43: p. 5372-5386
118. Leger C and Bertrand P (2008) Chem Rev 108: p. 2379-2438
119. Sharma R, Baik JH, Perera CJ, and Strano MS (2010) Nano Lett 10: p. 398-405
120. Zoski CG (2007) Handbook of electrochemistry. Elsevier, Amsterdam
121. Heller I, Kong J, Williams KA, Dekker C, and Lemay SG (2006) J Am Chem Soc 128: p. 7353-7359
122. Liang YY, Wang HL, Diao P, Chang W, Hong GS, Li YG, Gong M, Xie LM, Zhou JG, Wang J, Regier TZ, Wei F, and Dai HJ (2012) J Am Chem Soc 134: p. 15849-15857
123. Liang YY, Li YG, Wang HL, Zhou JG, Wang J, Regier T, and Dai HJ (2011) Nat Mater 10: p. 780-786
124. *Nomination profile: Hydroquinone*. 2009, U.S. Food & Drug Administration.
125. Deisinger PJ, Hill TS, and English JC (1996) J Toxicol Environ Health 47: p. 31-46
126. Zhao LS, Lin Y, Lao GH, Wang YC, Guan LJ, Wei JX, Yang ZX, Ni PY, Li X, Jiang ZY, Li T, Hao XY, Lin DT, Cao LP, and Ma XH (2015) J Affect Disorders 170: p. 85-90
127. Cha KH, Jensen GC, Balijepalli AS, Cohan BE, and Meyerhoff ME (2014) Anal Chem 86: p. 1902-1908
128. Andrade-Rocha FT (1999) Int Urol Nephrol 31: p. 107-11
129. Cui L, Peng Z, Ji C, Huang J, Huang D, Ma J, Zhang S, Qian X, and Xu Y (2014) Chem Commun 50: p. 1485-1487
130. Devasenathipathy R, Karuppiah C, Chen SM, Palanisamy S, Lou BS, Ali MA, and Al-Hemaid FMA (2015) RSC Adv 5: p. 26762-26768
131. Zhong AN, Luo XL, Chen LP, Wei SS, Liang YH, and Li XC (2015) Microchim Acta 182: p. 1197-1204
132. Chen HC, Tu YM, Hou CC, Lin YC, Chen CH, and Yang KH (2015) Anal Chim Acta 867: p. 83-91

133. Fu S, Fan GL, Yang L, and Li F (2015) Electrochim Acta 152: p. 146-154
134. Choi T, Kim SH, Lee CW, Kim H, Choi SK, Kim SH, Kim E, Park J, and Kim H (2015) Biosens Bioelectron 63: p. 325-330
135. Zhu X, Niu XH, Zhao HL, and Lan MB (2014) Sensor Actuat B-Chem 195: p. 274-280
136. Lin YQ, Li LB, Hu LL, Liu KY, and Xu YA (2014) Sensor Actuat B-Chem 202: p. 527-535
137. Deng SY, Zhang GY, Shan D, Liu YH, Wang K, and Zhang XJ (2015) Electrochim Acta 155: p. 78-84
138. Wang ML, Gao YQ, Zhang JJ, and Zhao JW (2015) Electrochim Acta 155: p. 236-243
139. Kutluay A and Aslanoglu M (2014) Anal Chim Acta 839: p. 59-66
140. Fei XM, Luo J, Liu R, Liu JC, Liu XY, and Chen MQ (2015) RSC Adv 5: p. 18233-18241
141. Wei C, Huang QT, Hu SR, Zhang HQ, Zhang WX, Wang ZM, Zhu ML, Dai PW, and Huang LZ (2014) Electrochim Acta 149: p. 237-244
142. Jiang YM, Jia LP, Yu SJ, and Wang CM (2014) J Mater Chem A 2: p. 6656-6662
143. Lai T, Cai WH, Dai WL, and Ye JS (2014) Electrochim Acta 138: p. 48-55
144. Devasenathipathy R, Mani V, and Chen SM (2014) Talanta 124: p. 43-51
145. Luo XL, Pan JB, Pan KM, Yu YY, Zhong AN, Wei SS, Li J, Shi JY, and Li XC (2015) J Electroanal Chem 745: p. 80-87
146. Kim SP and Choi HC (2015) Sensor Actuat B-Chem 207: p. 424-429
147. Li JH, Liu JL, Tan GR, Jiang JB, Peng SJ, Deng M, Qian D, Feng YL, and Liu YC (2014) Biosens Bioelectron 54: p. 468-475